Scilight

Regenerative Medicine and Dentistry
https://www.sciltp.com/journals/rmd

Article

TNFSF11 as a Key Regulator in Osteoarthritis Pathogenesis: Integrated Bioinformatics Analysis and Potential Therapeutic Targets

Fumin Yuan [1,2,†], Xiwei Fan [1,2,3,4,5,†], Indira Prasadam [3,4], Antonia Rujia Sun [3,4], Xiaoxin Wu [1,2,5], Yanping Wang [6,*] and Xinzhan Mao [1,2,5,*]

[1] Department of Orthopaedic Surgery, The Second Xiangya Hospital of Central South University, Changsha 410011, China
[2] Traumatic Orthopaedic Research Lab, The Second Xiangya Hospital of Central South University, Changsha 410011, China
[3] Centre for Biomedical Technologies, Queensland University of Technology, Brisbane, QLD 4059, Australia
[4] School of Mechanical, Medical & Process Engineering, Queensland University of Technology, Brisbane, QLD 4059, Australia
[5] National Clinical Research Centre for Metabolic Diseases, Department of Metabolism and Endocrinology, The Second Xiangya Hospital of Central South University, Changsha 410011, China
[6] Health Management Center, Xiangya Hospital of Central South University, Changsha 410028, China
* Correspondence: 1374715114@qq.com (Y.W.); Tel.: +86-135-7484-3486 (Y.W.); xinzhan.mao@csu.edu.cn (X.M.); Tel.: +86-139-7580-6781 (X.M.)
† These authors contributed equally to this work.

How To Cite: Yuan, F.; Fan, X.; Prasadam, I.; et al. TNFSF11 as a Key Regulator in Osteoarthritis Pathogenesis: Integrated Bioinformatics Analysis and Potential Therapeutic Targets. *Regenerative Medicine and Dentistry* **2026**, *3*(1), 4. https://doi.org/10.53941/rmd.2026.100004

Received: 26 January 2026
Revised: 2 March 2026
Accepted: 6 March 2026
Published: 19 March 2026

Abstract: Background: Osteoarthritis (OA) is a chronic joint disease marked by inflammation of the synovium, subchondral bone sclerosis, and cartilage deterioration. Although its underlying molecular mechanisms remain incompletely elucidated, tumour necrosis factor superfamily member 11 (TNFSF11) has been closely linked to the pathophysiology of OA. Elucidating the specific role of TNFSF11 may facilitate the development of novel diagnostic strategies and therapeutic interventions for OA. Methods: This study examined TNFSF11's function in OA using integrated bioinformatics. Transcriptome data of synovial tissues from OA patients and control (CON) subjects were retrieved from the Gene Expression Omnibus (GEO) database. The diagnostic value of TNFSF11 and differentially expressed genes (DEGs) was evaluated. TNFSF11-related genes were identified using weighted gene co-expression network analysis (WGCNA) and protein-protein interaction (PPI) analysis, results of which were confirmed by molecular docking. Immune cell infiltration and biological pathways were investigated using CIBERSORTx and functional enrichment analysis. TNFSF11-targeting medications were predicted using DrugBank. The causal associations between TNFSF11 and its target genes and OA were evaluated using two-sample Mendelian randomisation (MR) methodology. The expression of genes in clinical samples was verified using quantitative real-time polymerase chain reaction (qRT-PCR). Results: TNFSF11 was significantly upregulated in OA synovial tissues and demonstrated good diagnostic potential. A total of 372 TNFSF11-related genes were identified, among which 18 directly interacted with TNFSF11—findings that were validated by molecular docking. Functional enrichment was associated with immune response, cell adhesion, and matrix degradation pathways. TNFSF11 expression correlated with immune infiltration, particularly CD4 memory resting T cells, activated NK cells, and M0 macrophages. Four drugs (AMGN-0007, denosumab, lenalidomide, and thiocolchicoside) were predicted to target TNFSF11 with strong binding affinities. MR analysis revealed that CTSK, SPP1, and TBXAS1 were protective factors (all $p < 0.05$), while FCGR1A, MMP1, MMP9,

Copyright: © 2026 by the authors. This is an open access article under the terms and conditions of the Creative Commons Attribution (CC BY) license (https://creativecommons.org/licenses/by/4.0/).
Publisher's Note: Scilight stays neutral with regard to jurisdictional claims in published maps and institutional affiliations.

TNFRSF11A, and TNFSF11 were risk factors for OA (all $p < 0.05$). qRT-PCR validation confirmed significant upregulation of TNFSF11, TNFRSF11A, FCGR1A, MMP1, and MMP9 in OA samples (all $p < 0.05$), which was consistent with bioinformatics findings. Conclusions: TNFSF11 plays a critical role in OA pathogenesis by regulating target genes, immune cell infiltration, and inflammatory pathways. These findings offer novel insights into the function of TNFSF11 in OA and identify potential therapeutic targets for OA management.

Keywords: osteoarthritis; TNFSF11; WGCNA; PPI; immune infiltration; bioinformatics analysis; drug prediction

1. Introduction

Osteoarthritis (OA) is a complicated degenerative joint disease that results from complex interactions between various articular tissues and cellular components. It is characterised by progressive cartilage degradation, persistent synovial inflammation, subchondral bone remodelling, and osteophyte development [1]. Global epidemiological surveillance demonstrates escalating disease prevalence aligned with demographic aging. Notably, OA currently afflicts approximately 300 million individuals worldwide, imposing substantial socioeconomic burdens and profoundly compromising patient quality of life [2]. Despite extensive investigative efforts, key predisposing factors have been identified, including hereditary susceptibility, chronological aging, adiposity, and biomechanical joint malalignment [3]. However, the comprehensive molecular architecture underlying OA pathogenesis remains incompletely deciphered.

Disease progression involves convergent dysregulation across multiple biological axes: inflammatory cascades, chondrocyte metabolic perturbations, aberrant mechanotransduction, and extracellular matrix catabolism. The NF-κB axis orchestrates the expression of matrix-degrading proteases 4–6. These includeing matrix metalloproteinases (MMPs), with MMP-13 serving as a key mediator of type II collagen degradation, as well as aggrecanases of the ADAMTS family, particularly ADAMTS-5 [4–6]. IL-1β-mediated NF-κB activation amplifies pro-inflammatory cytokine production, thereby perpetuating tissue destruction [7,8]. Additionally, the Notch signalling pathway has also been found to enhance the expression of MMPs [9,10]. The JAK/STAT signalling pathway promotes chondrocyte apoptosis and synovial cell proliferation, sustains local inflammatory responses, and induces the secretion of MMPs [11–14]. The Wnt/β-catenin signalling pathway is excessively activated in OA, leading to chondrocyte hypertrophy, terminal differentiation, and mineralisation, ultimately disrupting cartilage structure [15–17]. The TGF-β signalling pathway promotes chondrocyte proliferation and maintains cartilage homeostasis at low concentrations [18]. However, at high concentrations, it can stimulate fibrosis and osteophyte formation [19,20]. Reactive oxygen species (ROS) activate oxidative stress responses [21–25]. Such responses damage chondrocyte DNA and proteins, induce chondrocyte apoptosis, and accelerate matrix degradation. A decline in autophagic function is a hallmark of OA progression. Impaired autophagy leads to the accumulation of organelles and metabolic waste, exacerbating cell death. The overactivation of the PI3K/Akt/mTOR signalling pathway inhibits autophagy and promotes cell death [26]. The Toll-like receptor (TLR) pathway promotes inflammation by releasing IL-1β and IL-18 [27]. Thus, there are currently no interventions to slow the progression of the disease [28]. Existing treatments primarily alleviate symptoms but cannot halt disease progression fundamentally. Therefore, exploring the molecular mechanisms of OA pathogenesis and identifying new therapeutic targets to enhance clinical treatment outcomes is crucial.

RANKL (TNFSF11) serves as a pivotal mediator of skeletal homeostasis by driving osteoclast maturation and activity. TNFSF11 triggers NF-κB signalling cascades, consequently upregulating osteoclastogenic gene expression programs [29]. Dysregulated TNFSF11 signalling contributes to osteoporosis, inflammatory arthropathies, and skeletal metastases [30–32]. Emerging evidence implicates TNFSF11 in OA pathophysiology, with elevated expression documented in diseased cartilage and synovium relative to healthy tissues [26,33]. TNFSF11 can stimulate the production of matrix-degrading enzymes in chondrocytes, such as MMPs and ADAMTS, leading to cartilage degradation [34]. In addition, TNFSF11 can promote the inflammatory response of OA by inducing the expression of pro-inflammatory cytokines and chemokines in synovial fibroblasts [35]. In OA animal models, inhibition of TNFSF11 signalling has been shown to alleviate cartilage degeneration and synovial inflammation [26]. These findings suggest that TNFSF11 may be a potential therapeutic target for OA. However, the comprehensive molecular mechanisms of TNFSF11 in the pathogenesis of OA and its relationship with other genes, pathways and microenvironment remain unclear, and its regulatory mechanisms require further elucidation.

Many factors affect joint and bone health, encompassing immunological networks, endocrine signalling, and microbial ecosystems. Immune surveillance primarily functions through the elimination of antigens and the maintenance of tissue equilibrium, serving as a critical guardian of physiological integrity. The innate immune system consists of cells and associated mechanisms that non-specifically resist infection [36]. During osteoarthritic pathogenesis, osteochondral elements engage in complex crosstalk with immunological mediators to preserve articular integrity. Inflammatory mediators cause tissue structural abnormalities in OA and aggravate OA cartilage damage [37,38]. Consequently, elucidating immune-cellular interactions across diverse tissue compartments during disease progression may unveil novel therapeutic approaches for OA management.

This investigation employed integrated transcriptomic analysis to dissect TNFSF11-centred molecular mechanisms in OA. We systematically assessed TNFSF11 expression profiles and diagnostic utility, identified disease-associated gene networks through differential expression screening and weighted co-expression network analysis (WGCNA), constructed protein interaction architectures, validated molecular partnerships via computational docking, characterised functional pathway enrichment, quantified immune cell infiltration patterns, and predicted candidate pharmacological agents through database mining with docking-based binding validation. Our multidimensional analytical framework illuminates TNFSF11's role in OA pathogenesis, identifies potential biomarkers and therapeutic targets, and establishes methodological paradigms applicable to the investigation of complex diseases.

2. Methods

2.1. Data Collection and Preprocessing

Three independent transcriptome datasets, including GSE55235, GSE55457, and GSE82107, which encompass synovial tissue specimens derived from OA patients and healthy individuals, were obtained from the Gene Expression Omnibus (GEO) database (accessible at https://www.ncbi.nlm.nih.gov/geo/ (accessed on 23 April 2024)). The first two datasets, GSE55235 and GSE55457, utilised the GPL96 microarray platform (Affymetrix Human Genome U133A Array, Affymetrix, Santa Clara, CA, USA), each comprising 10 osteoarthritic and 10 control specimens. The third dataset, GSE82107, utilised the GPL570 platform (Affymetrix Human Genome U133 Plus 2.0 Array, Affymetrix, Santa Clara, CA, USA) and comprised 10 disease and 7 healthy control samples. Initial data processing involved multiple standardisation steps, including background signal adjustment, probe-to-gene identifier mapping, and expression value normalisation. To enhance statistical robustness and analytical reliability, we integrated these three independent cohorts into a unified dataset using the "inSilicoMerging" package in the R programming environment. Technical variations arising from different experimental batches were addressed through the ComBat methodology, which simultaneously performed batch effect mitigation and median-centred normalisation across all datasets. The algorithm Robust Multi-array Average (RMA) was used for normalization. The effectiveness of this harmonisation procedure was confirmed through visual inspection of density distribution curves and dimensional reduction visualisation using the Uniform Manifold Approximation and Projection (UMAP) technique.

2.2. Expression Profiling and Diagnostic Performance Evaluation

To assess TNFSF11 transcript levels across OA and control (CON) cohorts, we employed the Wilcoxon rank-sum test for statistical comparison within each individual dataset (GSE55235, GSE55457, GSE82107) as well as the integrated cohort. Expression distributions were graphically depicted using box-and-whisker plots for intuitive visualisation. The discriminative ability of TNFSF11 as a potential biomarker for OA was systematically evaluated through the construction of receiver operating characteristic (ROC) curves. Diagnostic accuracy was quantified by calculating the area under the curve (AUC), a comprehensive metric that assesses the classifier's ability to differentiate between pathological and normal synovial tissues.

2.3. Identification of TNFSF11-Associated Genes in OA

A two-pronged strategy, integrating differential expression screening and weighted gene co-expression network analysis (WGCNA), was employed to identify genes functionally associated with TNFSF11 within the context of OA by leveraging a merged dataset. For the differential expression component, transcripts exhibiting substantial expression alterations between pathological and healthy specimens were filtered using stringent criteria: absolute fold change exceeding 1.5 and a statistical significance threshold of adjusted p-value < 0.05. The WGCNA methodology proceeded through a series of sequential computational steps. Initially, pairwise gene correlations were encoded in an adjacency matrix that quantified the strength of inter-node relationships.

Subsequently, an appropriate soft-thresholding power (β) was determined to convert this adjacency matrix into a topological overlap matrix, thereby establishing a scale-free network architecture characteristic of biological systems. Genes displaying coordinated expression profiles were aggregated into discrete modules through hierarchical clustering, complemented by a dynamic tree-cutting algorithm. To characterise the behaviour of individual modules, module eigengenes—serving as the primary principal component of each module's expression profile—were derived. Correlation analyses were subsequently performed to assess relationships between each module and two variables: disease status and the abundance of TNFSF11 transcripts. Modules demonstrating significant simultaneous correlations with disease phenotype and TNFSF11 expression were prioritised for subsequent investigation. The final candidate gene set was derived by intersecting module-resident genes with differentially expressed transcripts, yielding TNFSF11-associated genes specific to the pathophysiology of OA.

2.4. Protein-Protein Interaction (PPI) Network Construction

To elucidate the regulatory networks centred on TNFSF11 in OA, we mapped protein interactions for candidate genes from Section 2.3 using the STRING database (https://string-db.org/ (accessed on 27 April 2024)). The network topology was visualised with Cytoscape software (version 3.8.2; The Cytoscape Consortium, New York, NY, USA), highlighting direct binding partners and indirect functional associates of TNFSF11. These direct interactors were validated using several methods, including comparing expression levels between OA and CON groups via the Wilcoxon rank-sum test, assessing coordinated expression with Pearson correlation coefficients, and evaluating diagnostic potential through ROC curve analysis.

2.5. Protein-Protein Interaction Validation via Molecular Docking

To computationally validate predicted protein associations from the interaction network, we performed in silico docking simulations between TNFSF11 and its putative binding partners (BLNK, CD4, CSF1R, CTSK, FCGR1A, FCGR3A, FCGR3B, MMP1, MMP3, MMP9, OGN, SDC1, SPP1, TBXAS1, TNFRSF11A, TYROBP, VCAM1, TREM2). The three-dimensional crystallographic coordinates of all proteins were acquired from the RCSB Protein Data Bank (https://www.rcsb.org/ (accessed on 29 April 2024)). Docking was performed using the HDOCK web server (http://hdock.phys.hust.edu.cn/ (accessed on 11 May 2024)) following the validated protocol of Yan et al. [39]. Simulation parameters included human species specification, physiological pH (7.4), and the balanced scoring function implemented within HDOCK, with all remaining settings retained at server defaults. Binding interaction strength was evaluated using the HDOCK dimensionless docking score, where increasingly negative values reflect a higher predicted likelihood of interaction; critically, these scores represent a computational scoring function output and must not be interpreted as binding free energies in kcal/mol. Docking reliability was assessed using the confidence score (values >0.7 indicate reliable predictions). Molecular interaction interfaces of the five top-ranked complexes were visualised using PyMOL (version 2.3; Schrödinger, LLC, New York, NY, USA), enabling detailed examination of hydrogen bonds, hydrophobic contacts, and van der Waals interactions.

2.6. Functional Enrichment and Pathway Analysis

To clarify the biological mechanisms and molecular signalling pathways associated with TNFSF11 in the development of OA, we performed systematic functional annotation of genes within the protein-protein interaction network using the DAVID (Database for Annotation, Visualisation and Integrated Discovery) bioinformatics resource (https://david.ncifcrf.gov/ (accessed on 27 May 2024)). Significantly enriched Gene Ontology (GO) terms—including biological processes, cellular components, and molecular functions—along with Kyoto Encyclopedia of Genes and Genomes (KEGG) pathways were identified using a statistical cutoff of $p < 0.05$. Additionally, complementary gene set enrichment analysis (GSEA) was performed to confirm the differential activation of these pathways between the comparison groups. OA specimens were divided into high- and low-TNFSF11 expression groups based on the median expression value as the cut-off. Enrichment analyses were performed for two separate comparisons: disease versus control specimens, and TNFSF11-high versus TNFSF11-low OA samples. The analysis utilised the "GSEA" R package, with previously identified KEGG pathways serving as reference gene sets. The significance of pathway activation was evaluated through normalised enrichment scores (NES) along with their *p*-values.

2.7. Immune Cell Infiltration Profiling

To characterise the immune landscape within synovial tissues, we employed CIBERSORTx (https://cibersortx.stanford.edu/ (accessed on 27 April 2024)), a computational deconvolution method that leverages machine learning algorithms to infer the relative abundances of 22 distinct immune cell populations from bulk transcriptomic profiles. This approach enabled quantitative assessment of immune cell composition across individual OA and control specimens. Statistical comparison of cellular infiltration patterns between disease and healthy cohorts was conducted using the Wilcoxon rank-sum test. Additionally, Pearson correlation coefficients were calculated to investigate intercellular relationships among immune populations and to assess the associations between TNFSF11 expression levels and the frequencies of individual immune cell subsets.

2.8. Drug Prediction and Molecular Docking Validation

Candidate pharmacological agents targeting TNFSF11 were identified through systematic interrogation of the DrugBank database (https://go.drugbank.com/ (accessed on 22 August 2024)). Computational docking simulations were subsequently performed to assess binding feasibility between predicted compounds and TNFSF11. Candidate drugs were assessed for binding to TNFSF11 using two approaches matched to drug type. For the macromolecular therapeutic agents denosumab and AMGN-0007, protein–protein docking was performed using the HDOCK web server 39, following identical protocols to those described in Section 2.5; binding interaction likelihood was quantified by the HDOCK dimensionless docking score. For the small-molecule candidates lenalidomide and thiocolchicoside, docking simulations were also conducted via HDOCK to allow direct score comparability across all four candidates; HDOCK output values are dimensionless and do not represent kcal/mol free energies. Interaction interfaces for all top-ranked complexes were visualised using PyMOL (version 2.3; Schrödinger, LLC, New York, NY, USA), and key stabilising contacts (hydrogen bonds, hydrophobic interactions, van der Waals forces) were characterised to inform the therapeutic potential of each candidate against TNFSF11.

2.9. Mendelian Randomization Analysis

To evaluate potential causal relationships between gene expression and OA susceptibility, we performed two-sample Mendelian randomisation (MR) analysis. Genome-wide association study (GWAS) summary statistics for osteoarthritis outcome data were retrieved from the OpenGWAS repository (https://gwas.mrcieu.ac.uk/ (accessed on 30 April 2025)), specifically from dataset ukb-b-14486, which encompasses 424,461 healthy individuals and 38,472 affected patients. Exposure variables comprised gene expression levels derived from blood expression quantitative trait loci (eQTL) datasets provided by the eQTLGen Consortium (31,684 participants). Seventeen candidate genes underwent MR examination: SPP1, TREM2, FCGR1A, TBXAS1, CSF1R, TYROBP, MMP9, TNFRSF11A, FCGR3B, FCGR3A, MMP1, VCAM1, BLNK, CTSK, CD4, SDC1, and TNFSF11. Genetic instruments were selected through stringent quality filters: (1) genome-wide significant gene-expression associations ($p < 5 \times 10^{-8}$); (2) independence assured via linkage disequilibrium pruning ($r^2 < 0.001$, 10,000 kb windows); (3) instrument strength verified by F-statistics exceeding 10; and (4) pleiotropic variants directly influencing OA risk ($p < 5 \times 10^{-8}$) were excluded. The inverse variance weighted (IVW) approach constituted the primary analytical framework.

2.10. Clinical Sample Collection and Quantitative Real-Time PCR Validation

Synovial tissue specimens were prospectively collected from patients undergoing surgical procedures at The Second Xiangya Hospital of Central South University. Ethical approval for this experiment was obtained from the Ethics Committee of the Second Xiangya Hospital of Central South University, and all participants provided informed consent (Human Ethics Number: KYZ20250159). The study cohort comprised 10 patients with primary knee OA and 10 control (CON) patients without OA (Detailed demographic data was shown in Table S1). For the OA group, inclusion criteria were: (1) age ≥ 45 years; (2) diagnosis of primary knee OA according to American College of Rheumatology (ACR) criteria; (3) Kellgren-Lawrence radiographic grade ≥ 2; and (4) scheduled for knee arthroscopy or total knee arthroplasty. For the control group, inclusion criteria were: (1) age ≥ 45 years; (2) undergoing arthroscopic surgery for traumatic meniscal tears or anterior cruciate ligament injuries; (3) no clinical or radiographic evidence of OA (Kellgren-Lawrence grade 0); and (4) no history of inflammatory joint diseases. Exclusion criteria for both groups included secondary OA, inflammatory arthropathies, intra-articular corticosteroid injections within 3 months, systemic corticosteroid or immunosuppressive therapy within 6 months, active malignancy or history of cancer within 5 years, severe hepatic or renal dysfunction, infectious diseases, and previous knee surgery on the same joint within 1 year. Synovial tissue samples (approximately 50–100 mg) were

obtained from the suprapatellar pouch region during surgery, immediately snap-frozen in liquid nitrogen, and stored at −80 °C until analysis. Total RNA was extracted using TRIzol reagent (Invitrogen, Thermo Fisher Scientific, Waltham, MA, USA), with RNA quality assessed by spectrophotometry (A260/A280 ratio 1.8–2.0). First-strand cDNA synthesis was performed using the PrimeScript RT reagent kit (Takara Bio Inc., Kusatsu, Japan) with 1 μg total RNA. Quantitative real-time PCR was conducted using TB Green Premix Ex Taq (Takara Bio Inc., Kusatsu, Japan) with the following thermal cycling conditions: initial denaturation at 95 °C for 30 s, followed by 40 cycles of 95 °C for 5 s and 60 °C for 30 s. Each sample was analyzed in triplicate, and melting curve analysis verified amplification specificity. Primer sequences for target genes (TNFSF11, TNFRSF11A, FCGR1A, MMP1, MMP9) and the endogenous reference gene GAPDH are provided in Supplementary Materials Table S2. Relative gene expression levels were calculated using the $2^{-\Delta\Delta Ct}$ method with GAPDH normalization. Statistical comparisons between groups were performed using independent t-tests for normally distributed data or Mann-Whitney U tests for non-normally distributed data, with $p < 0.05$ considered statistically significant.

3. Results

3.1. Integration Quality Assessment of Multi-Cohort Transcriptomic Data

Following computational harmonisation of the three independent datasets (GSE55235, GSE55457, and GSE82107), we evaluated integration quality through multiple visualisation approaches. Density distribution analyses (Figure 1A,B) demonstrated substantial convergence of expression profiles across batches, with individual sample distributions exhibiting high concordance regardless of original cohort assignment. Dimensional reduction via UMAP (Figure 1C,D) further confirmed successful integration, revealing thorough intermixing of specimens from distinct experimental batches without discernible batch-driven segregation patterns. These quality metrics validated the efficacy of the ComBat harmonisation algorithm, establishing a unified analytical framework comprising 30 osteoarthritic and 27 healthy synovial specimens suitable for downstream comparative investigations.

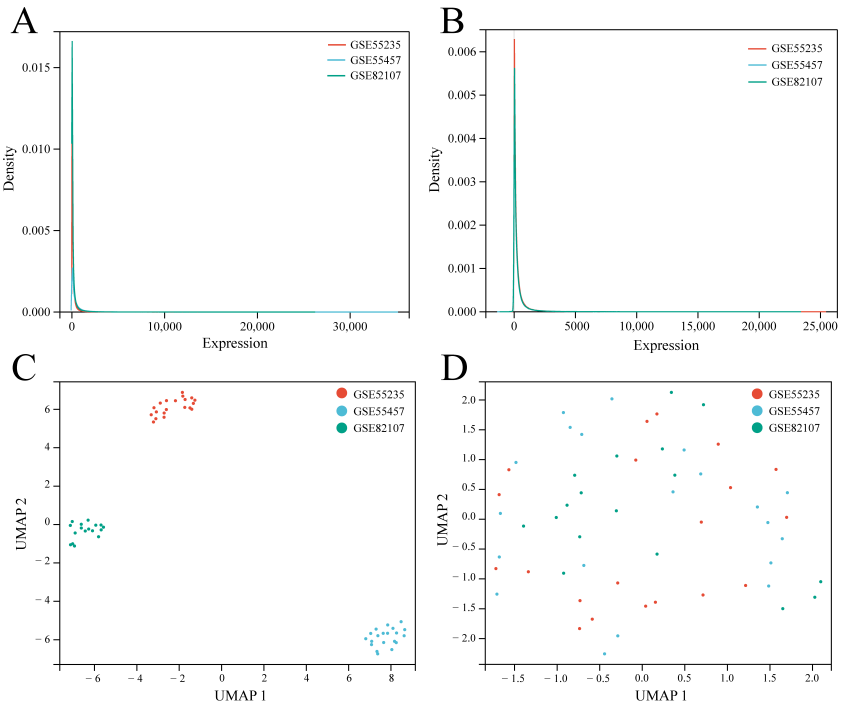

Figure 1. Evaluation of batch effect correction for integrated datasets. (**A**) Density distribution of the sample expression before correction in different batches. (**B**) Density distribution of the sample expression after correction in different batches. (**C**) UMAP plot of all samples before correction. (**D**) UMAP analysis of all samples after removing batch effects.

3.2. Differential Expression and Diagnostic Value of TNFSF11

TNFSF11 expression levels were significantly elevated in OA samples relative to control specimens across the GSE55235, GSE55457, and GSE82107 datasets, as well as the integrated dataset ($p < 0.05$) (Figure 2A–D). ROC curve analysis demonstrated that the AUC values of TNFSF11 for OA diagnosis were 1.00, 0.780, 0.800,

and 0.878 in GSE55235, GSE55457, GSE82107, and the integrated dataset, respectively (Figure 2E–H), suggesting that TNFSF11 exhibits high diagnostic utility for OA.

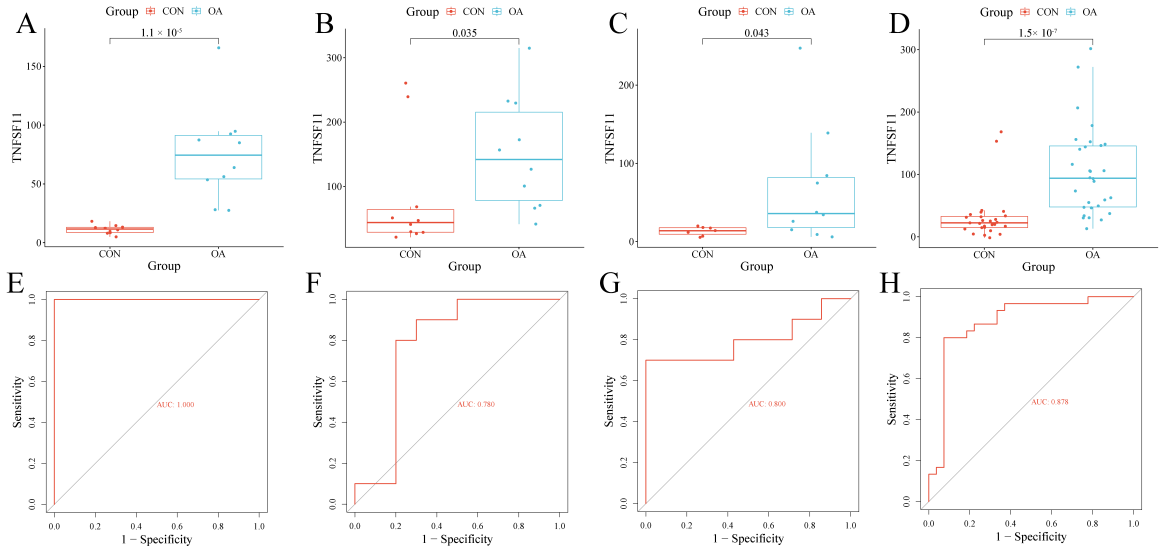

Figure 2. Differential expression and diagnostic value analysis of TNFSF11 in OA and CON synovial tissues. (**A**) Differential expression analysis of TNFSF11 based on GSE55235. (**B**) Differential expression analysis of TNFSF11 based on GSE55457. (**C**) Differential expression analysis of TNFSF11 based on GSE82107. (**D**) Differential expression analysis of TNFSF11 based on the integrated dataset. (**E**–**H**) ROC curve analyses assessing TNFSF11 diagnostic performance for OA across GSE55235 (**E**), GSE55457 (**F**), GSE82107 (**G**), and the integrated cohort (**H**). The statistical analysis was performed using the Wilcoxon rank-sum test for the abovementioned comparison ($p < 0.05$).

3.3. Identification of TNFSF11-Related Genes in OA

Differential expression screening revealed 1432 transcripts exhibiting significant abundance changes between disease and control cohorts (751 elevated, 681 reduced in OA; |fold change| > 1.5, adjusted $p < 0.05$) (Figure 3A,B). For weighted co-expression network construction, a soft-thresholding power β of 9 was selected to achieve a scale-free topology (Figure 3C). Implementing the DynamicTreeCut algorithm with parameters (minimum module membership: 30 genes; split sensitivity: 3; merge threshold: 0.25), we identified 25 distinct co-expression modules designated by colour nomenclature: midnight blue, dark orange, red, dark green, dark turquoise, royal blue, saddle brown, light cyan, cyan, dark magenta, orange, green yellow, light yellow, pale turquoise, brown, turquoise, pink, blue, grey60, dark olive green, black, dark red, light green, steel blue, and grey (Figure 3D). Eigengene network analysis confirmed module independence, with inter-module distances exceeding 0.25 (Figure 3E). Correlation profiling between module eigengenes and both disease status and TNFSF11 transcript levels identified six modules (blue, cyan, pink, grey, saddle brown) demonstrating dual significant associations (|r| > 0.5, $p < 0.05$), collectively encompassing 1318 transcripts (Figure 3F). Intersection of these module constituents with differentially expressed genes yielded 372 candidate genes representing the TNFSF11-associated transcriptional signature in OA (Figure 3G).

3.4. PPI Network of TNFSF11-Related Genes

Protein interaction mapping of the OA-associated gene set generated a network comprising 280 protein nodes interconnected through 1450 documented associations (Figure 4A). Network topology analysis distinguished 18 proteins exhibiting immediate functional or physical linkage to TNFSF11 (BLNK, CD4, CSF1R, CTSK, FCGR1A, FCGR3A, FCGR3B, MMP1, MMP3, MMP9, OGN, SDC1, SPP1, TBXAS1, TNFRSF11A, TYROBP, VCAM1, TREM2), while the remaining 268 nodes represented secondary-tier interactors, implying multi-level regulatory cascades potentially orchestrated by TNFSF11 during OA pathogenesis. Expression profiling of the 18 direct TNFSF11 partners revealed consistent upregulation in diseased versus healthy synovium ($p < 0.05$) (Figure 4B). Co-expression analysis revealed predominantly positive correlations among these proteins, with TNFSF11 exhibiting coordinated expression patterns with all partners, except for FCGR3 ($p < 0.05$, $R > 0$) (Figure 4C). Diagnostic performance evaluation via receiver operating characteristic analysis confirmed the discriminatory capacity of these direct interactors, with each achieving an area under the curve value exceeding 0.6 (Figure 4D).

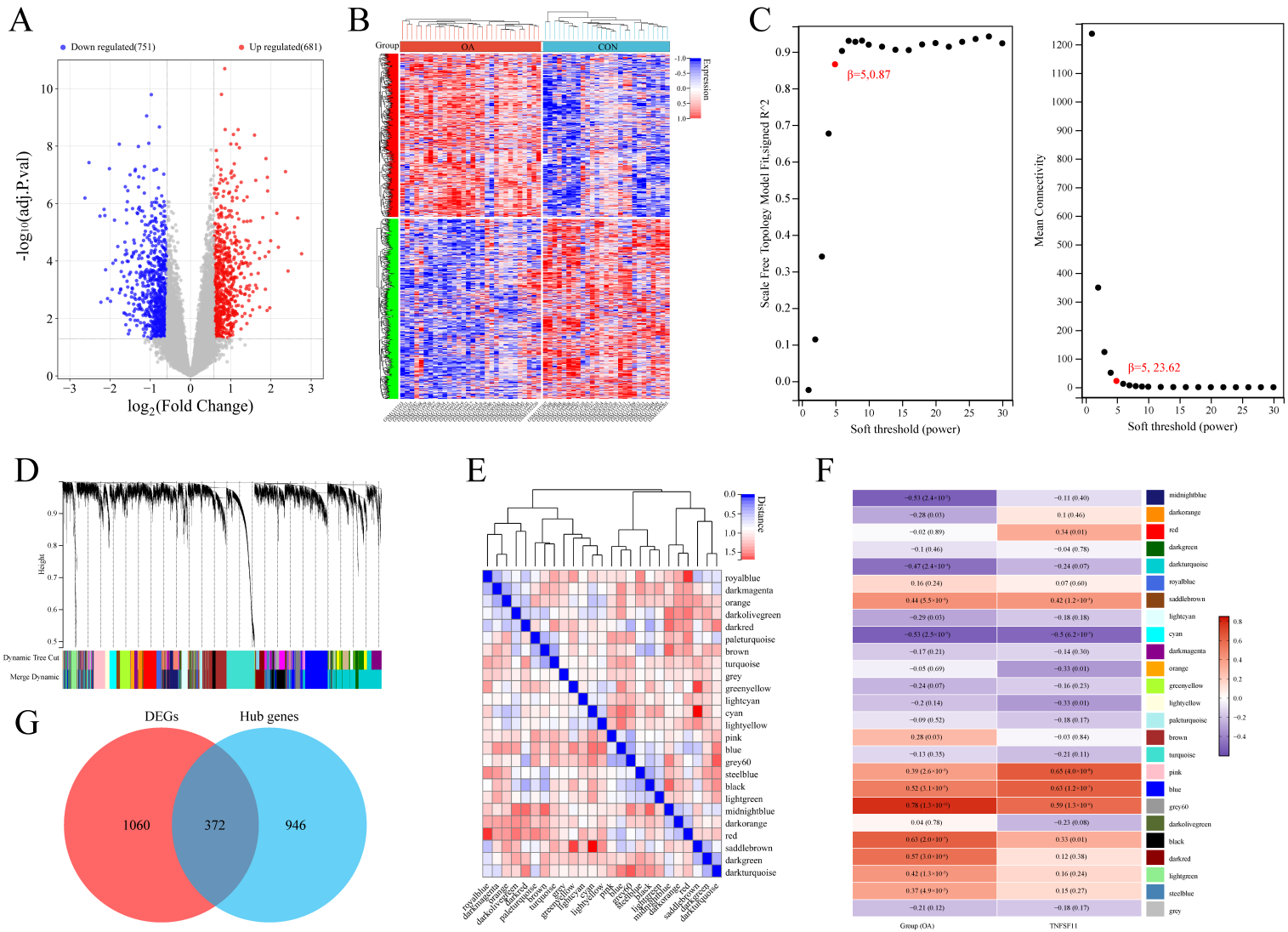

Figure 3. Screening of TNFSF11 co-expressed genes in OA. (**A**) Volcano plot showing DEGs between OA and CON groups. 681 genes were up-regulated and 751 genes were down-regulated in OA group. (**B**) Heatmap of DEGs in OA and CON samples. (**C**) Relationship between different soft thresholds (power values) and the fitting index R^2 (y-axis) and mean connectivity (mean node degree, x-axis) of the network. (**D**) Gene clustering tree and co-expression module division. (**E**) Clustering diagram of module eigengenes (MEs) and connectivity heatmap between modules. The colour intensity of each square represents the strength of connectivity between corresponding modules. (**F**) Heatmap of correlations between MEs, clinical traits, and TNFSF11 expression. (**G**) Screening of TNFSF11 co-expressed genes.

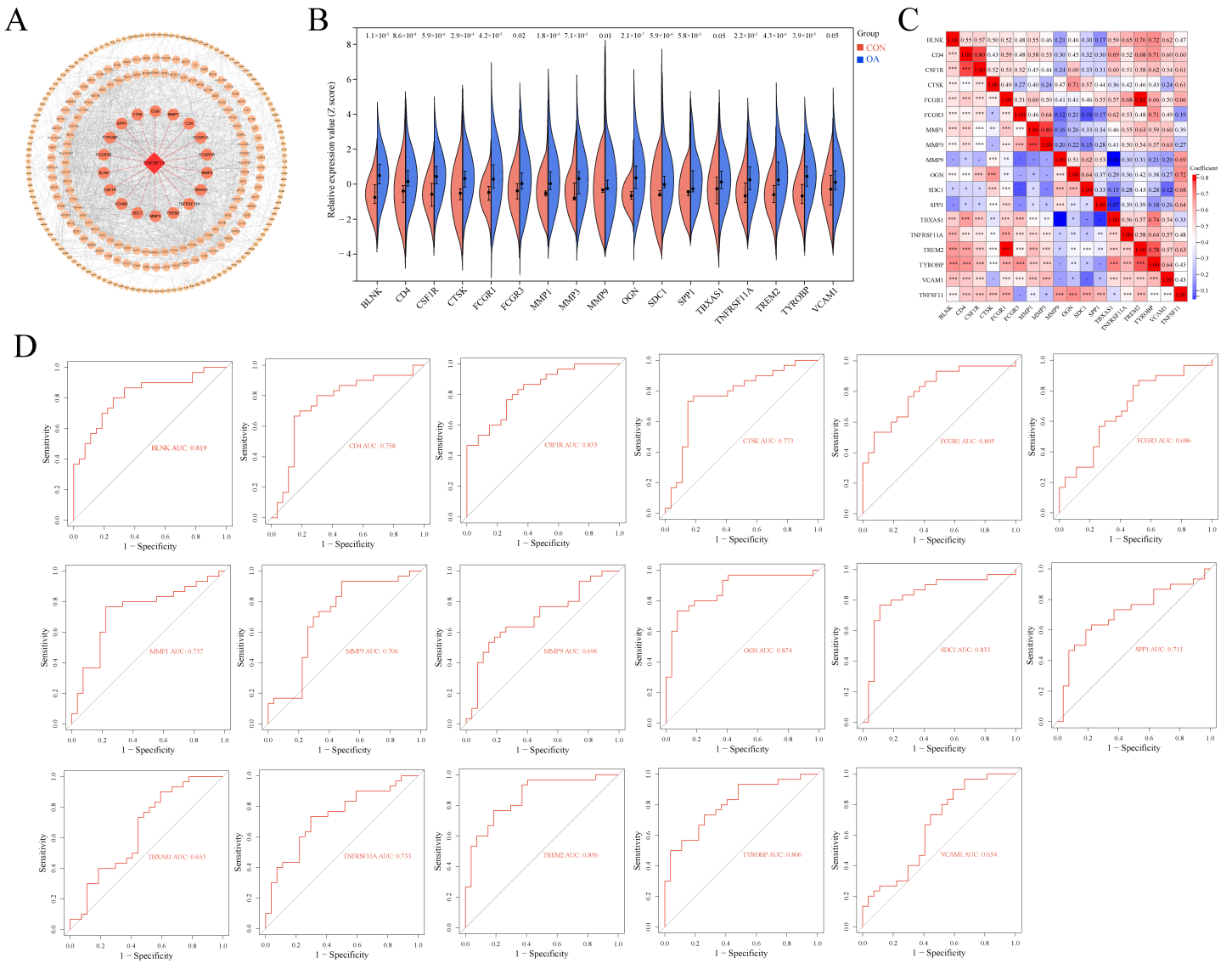

Figure 4. PPI network analysis. (**A**) PPI network of TNFSF11 co-expressed genes in OA. Circular nodes represent TNFSF11 co-expressed genes, edges represent interaction relationships, and red edges indicate direct interaction with TNFSF11. (**B**) Differential expression analysis of genes directly interacting with TNFSF11 in OA and CON groups. Wilcoxon rank-sum test. (**C**) Heatmap of expression correlations between TNFSF11 and its directly interacting genes. *$p < 0.05$, **$p < 0.01$, ***$p < 0.001$. Pearson correlation. (**D**) ROC curve plot of genes directly interacting with TNFSF11.

3.5. Computational Validation of TNFSF11-Target Protein Interactions

Molecular docking simulations confirmed predicted binding interactions between TNFSF11 and all 18 direct partners. The HDOCK docking scores, which reflect the statistical likelihood of interaction rather than thermodynamic binding affinity, spanned −226.19 to −432.54, with all complexes achieving confidence scores exceeding 0.8 (Table 1).

A detailed structural analysis of the five highest-affinity complexes elucidated the molecular recognition mechanisms. The TNFSF11-SPP1 interface exhibited five hydrogen-bonding interactions involving TNFSF11 residues S260, S265, N267 and SPP1 residues F293, Y290, K289. TNFSF11-TREM2 complex formation engaged eight hydrogen bonds linking TNFSF11 residues N276, S274, Y273, T261, K262, Y263, S268, H271 with TREM2 residues F74, W78, R98, S31, T94, Q33. TNFSF11-MMP3 association featured ten hydrogen bonds connecting TNFSF11 residues R314, Y215, Y307, N276 to MMP3 residues T85, N162, P160. Similarly, the TNFSF11-FCGR1A binding interface comprised ten hydrogen bonds between TNFSF11 residues A162, K195, H167, A128, V277, Y307, N276, N219, R223, S268 and FCGR1A residues S51, E44, Q27, L26, T154, K145. TNFSF11-TBXAS1 interaction involved three hydrogen bonds formed by TNFSF11 residues S260, S274 and TBXAS1 residues K48, S50 (Figure 5). These structural findings corroborate the protein interaction network predictions, providing atomic-level evidence for TNFSF11-mediated regulatory circuits.

Table 1. Molecular docking results between TNFSF11 and its direct target.

Genes	Docking Score	Confidence Score	Ligand rmsd (Å)
SPP1	−432.54	0.9965	28.02
TREM2	−373.6	0.9835	59.83
MMP3	−357.37	0.9844	27.71
FCGR1A	−340.19	0.9782	33.79
TBXAS1	−328.49	0.9726	30.93
CSF1R	−327.63	0.9721	15.51
TYROBP	−323.96	0.9701	44.09
MMP9	−303.42	0.9556	49.03
OGN	−302.56	0.9548	53.43
TNFRSF11A	−298.3	0.951	30.03
FCGR3B	−298.22	0.9509	9.89
FCGR3A	−295.96	0.9488	70.22
MMP1	−283.23	0.9349	67.38
VCAM1	−268.4	0.9144	61.58
BLNK	−267.14	0.9124	30.26
CTSK	−261.74	0.9033	69.41
CD4	−256.7	0.8942	68.02
SDC1	−226.19	0.8211	35.59

3.6. Functional Enrichment Analysis

To further investigate the biological functions involved in the role of TNFSF11 in the development of OA, we performed functional enrichment analysis on the genes potentially regulated by TNFSF11 in the PPI network. GO enrichment analysis revealed that these genes were primarily implicated in 145 biological processes (biological processes, BP), including but not limited to positive modulation of T lymphocyte activation, antigen processing and presentation of peptide or polysaccharide antigens through major histocompatibility complex (MHC) class II molecules, antigen processing and presentation of exogenous peptide antigens via MHC class II molecules, assembly of peptide antigens into MHC class II protein complexes, and cellular adhesion (Figure 6A). These genes were predominantly localised to cellular components (CC), encompassing the extracellular region, extracellular space, extracellular exosome, lysosomal lumen, and extracellular matrix (Figure 6B). At the molecular function (MF) level, these genes were associated with 36 functions, such as extracellular matrix structural constituent, heparin-binding, MHC class II protein complex binding, receptor binding, and MHC class II receptor activity (Figure 6C). KEGG enrichment analysis revealed that the genes directly or indirectly interacting with TNFSF11 in OA were mainly enriched in 20 signalling pathways, including phagosome, cell adhesion molecules, lysosome, Fc gamma R-mediated phagocytosis, NOD-like receptor signalling pathway, and hematopoietic cell lineage (Figure 6D,E). GSEA demonstrated that the expression profiles of various KEGG signalling pathways exhibited significant differences between the OA group and the CON group, as well as between the TNFSF11 high-expression group and the TNFSF11 low-expression group. Notably, several signalling pathways, including phagosome, cell adhesion molecules, lysosome, protein digestion and absorption, leukocyte transendothelial

migration, hematopoietic cell lineage, and intestinal immune network for IgA production, were markedly upregulated in OA synovial tissues relative to CON synovial tissues, and similarly in OA synovial tissues with high TNFSF11 expression compared to those with low TNFSF11 expression. Conversely, certain signalling pathways, such as the insulin signalling pathway and the regulation of lipolysis in adipocytes, were notably decreased in OA synovial tissues when compared to healthy counterparts, and in OA synovial tissues with high TNFSF11 expression versus those with low TNFSF11 expression (Figure 6F,G).

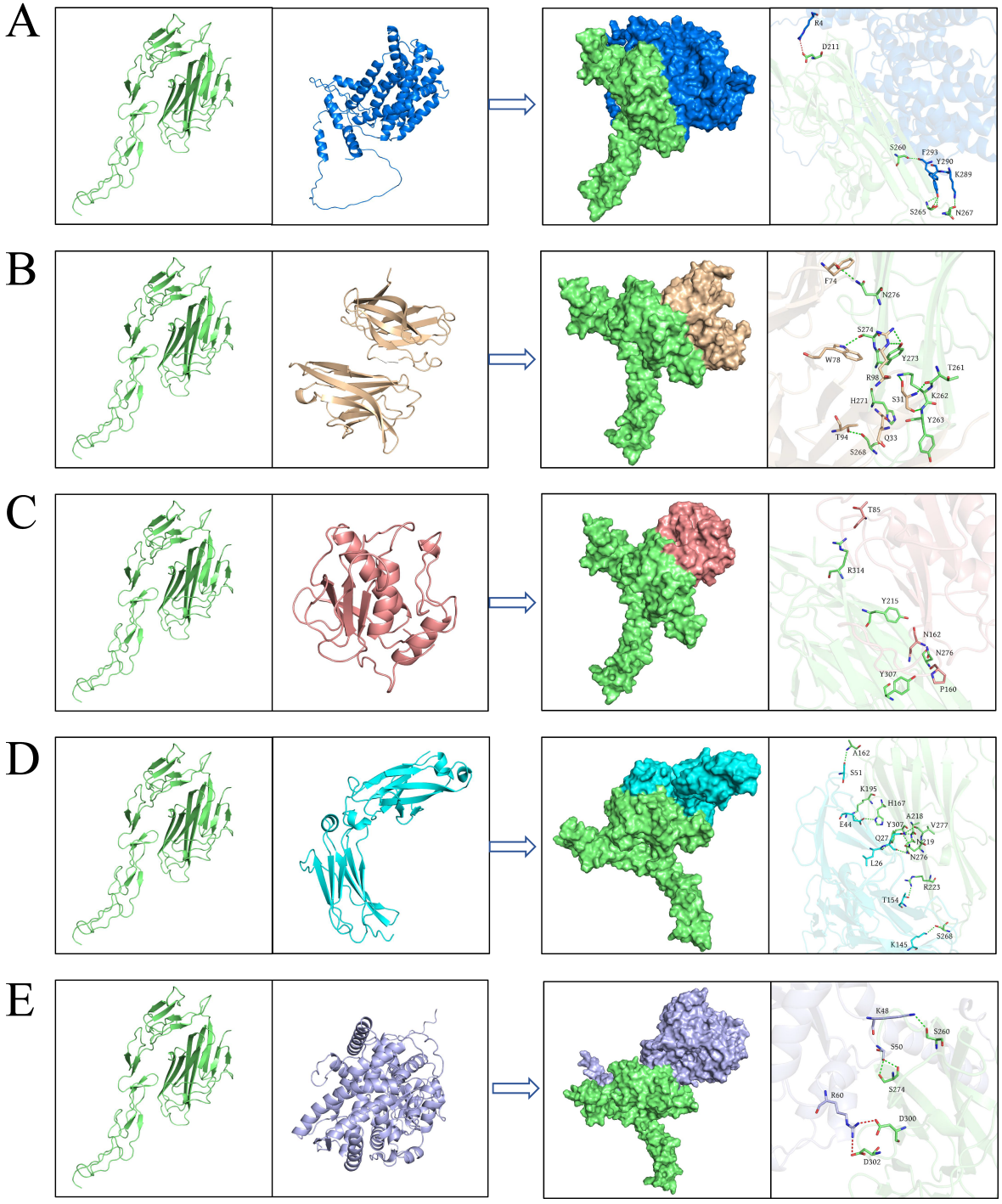

Figure 5. Molecular docking simulation of TNFSF11 with its directly interacting targets. Three-dimensional structural models of TNFSF11 complexes with SPP1 (**A**); TREM2 (**B**); MMP3 (**C**); FCGR1A (**D**); and TBXAS1 (**E**). TNFSF11 depicted in green with critical residues shown as sticks; green dashes indicate hydrogen bonds; red dashes denote salt bridges.

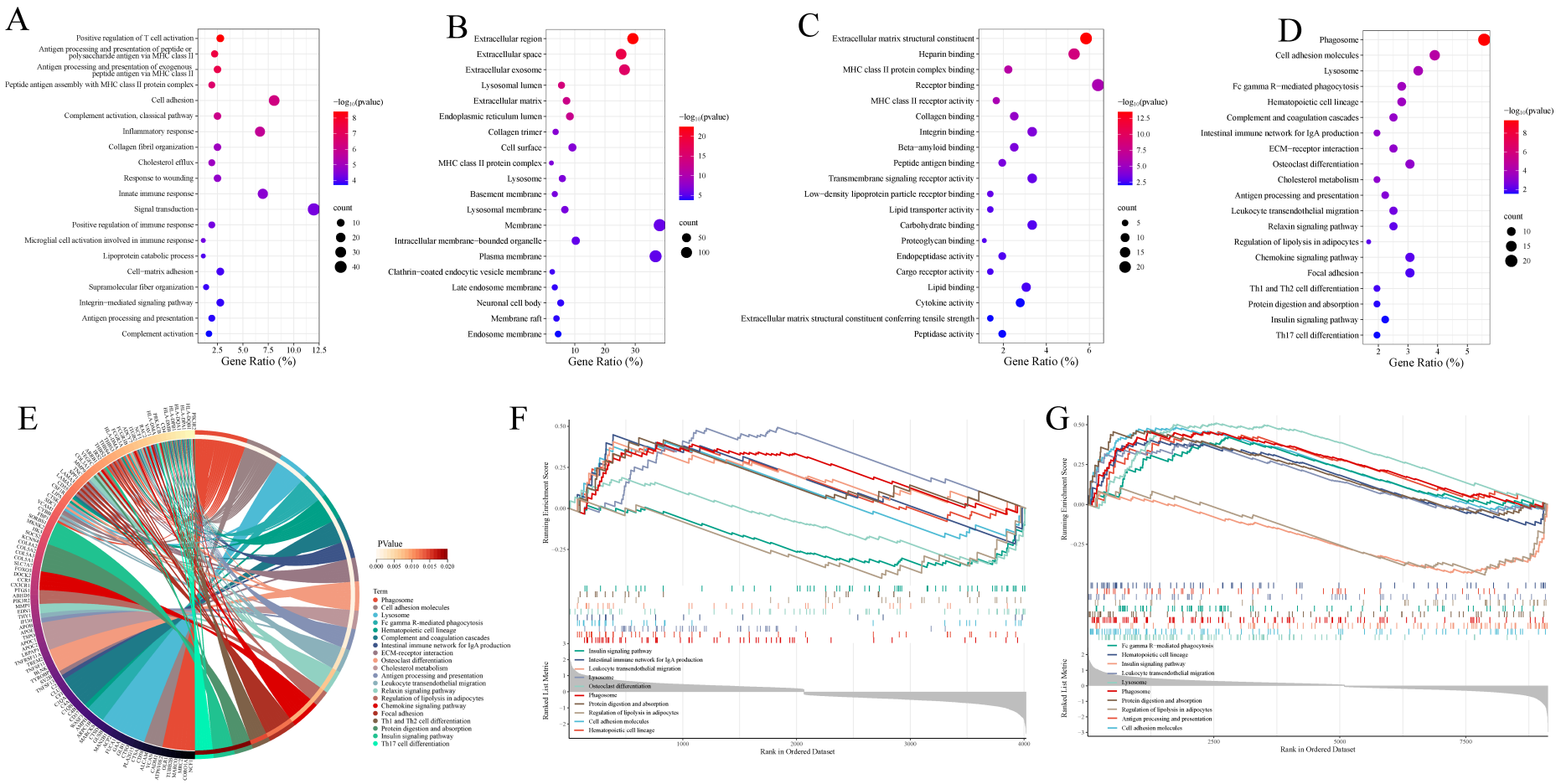

Figure 6. Functional enrichment analysis. (**A**) Bubble plots of enriched BP. (**B**) Bubble plots of enriched CC. (**C**) Bubble plots of enriched MF**.** GO terms for TNFSF11 co-expressed genes (top 20 terms with the highest significance). (**D**) Bubble plot of enriched KEGG pathways for TNFSF11 co-expressed genes. (**E**) Connection relationship between TNFSF11 co-expressed genes and enriched KEGG pathways. (**F**) GSEA identifies significantly differentially expressed signalling pathways between OA and CON groups (top 10 KEGG signalling pathways with the highest significance). (**G**) GSEA identifies significantly differentially expressed signalling pathways between high and low TNFSF11 expression groups in OA synovial tissues (Top 10 KEGG signalling pathways with the highest significance).

3.7. Immune Infiltration Profiling

Computational deconvolution quantified 22 distinct immune cell populations across tissue specimens. Bar plots and heatmaps illustrated cellular composition and abundance patterns for individual samples (Figure 7A,B). Inter-cellular correlation analysis (Figure 7C) revealed strong positive associations between T cells, CD4 naive, and NK cells resting (R = 0.77), contrasting with clear negative relationships between resting and activated Mast cells (R = −0.67).

Comparative analysis of immune landscape differences between OA and control synovium showed significant enrichment of naive B cells, T cells regulatory (Tregs), Macrophages M0, and Mast cells resting in diseased tissues, whereas T cells CD4 memory resting, Mast cells activated, NK cells resting, and Eosinophils showed marked depletion in osteoarthritic synovium (Figure 7D). Correlation profiling between TNFSF11 transcript levels and cellular infiltration patterns uncovered inverse associations with T cells, CD4+ memory resting cells, and NK cells, as well as positive correlations with M0 macrophage abundance (Figure 7E).

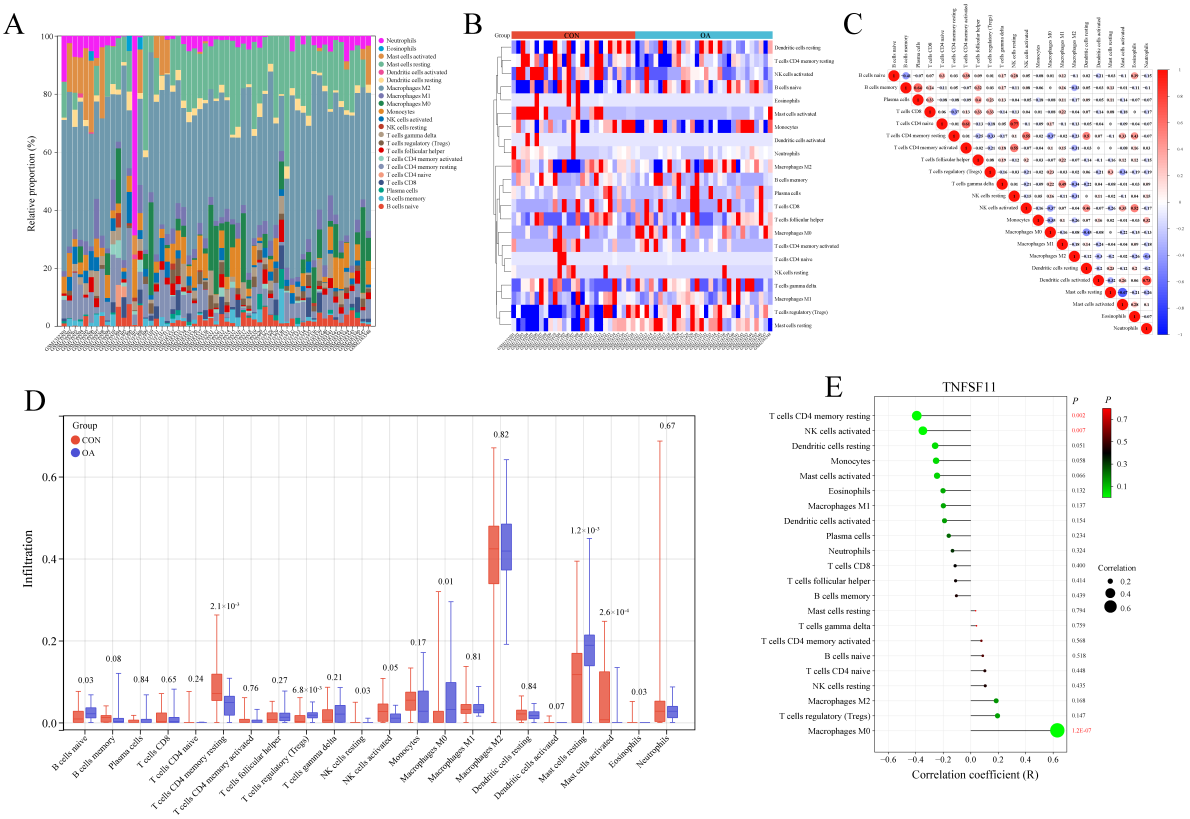

Figure 7. Immune cell landscape characterization in osteoarthritic synovium via CIBERSORTx deconvolution. (**A**) Bar chart depicting cellular composition across specimens. (**B**) Heatmap illustrating abundance patterns of 22 leukocyte populations. (**C**) Heatmap of pairwise correlations among 22 immune cell subsets. Pearson correlation. (**D**) Differential analysis of immune cell subset infiltration between OA and CON groups. Wilcoxon rank-sum test. (**E**) Bubble plot of correlations between TNFSF11 expression and immune cell infiltration. Pearson correlation.

3.8. Drug Prediction and Molecular Docking Validation

Using the DrugBank database, four potential targeted drugs for TNFSF11 were identified, including Denosumab, AMGN-0007, Lenalidomide, and Thiocolchicoside. Denosumab is already a monoclonal antibody targeting RANKL—specifically, a fully humanized monoclonal neutralizing antibody belonging to the IgG2 subclass of immunoglobulins Its development stemmed from in-depth exploration of the OPG-RANK-RANKL pathway [40,41]. *In vitro* studies show that, much like OPG, denosumab binds both soluble and membrane-bound RANKL with high affinity. This allows it to competitively attach to RANKL, blocking its interaction with the RANK receptor[42]. This binding mechanism goes on to inhibit the differentiation, survival, and activity of osteoclasts—ultimately suppressing osteoclast-mediated bone resorption and helping regulate bone metabolism [43]. Denosumab also boasts favorable pharmacokinetic properties. It's quickly absorbed after subcutaneous injection, has a nonlinear metabolic pattern, and maintains effective *in vivo* concentrations for an extended period—its half-life is roughly 26 to 28 days [44,45]. Its identification by our pipeline serves as an important positive control,

validating the reliability of our prediction method. Molecular docking results indicated that the small molecule drugs lenalidomide and thiocolchicoside, along with the macromolecular drugs AMGN-0007 and denosumab, showed good binding interactions with TNFSF11 (Figure 8). The docking scores of Denosumab, AMGN-0007, Lenalidomide, and Thiocolchicoside with TNFSF11 were −8.27, −7.85, −412.35 and −490.42, respectively. These are dimensionless HDOCK scoring function values reflecting predicted interaction likelihood, not binding free energies in kcal/mol. Hydrogen bonds, hydrophobic interactions, and van der Waals forces between the drugs and the key residues in the binding pocket of TNFSF11 stabilised the docked complexes. These findings suggest that these four drugs might have therapeutic effects on OA by targeting TNFSF11. Denosumab further confirms that our predictions are quite stable, and the remaining three drugs are likely to be effective.

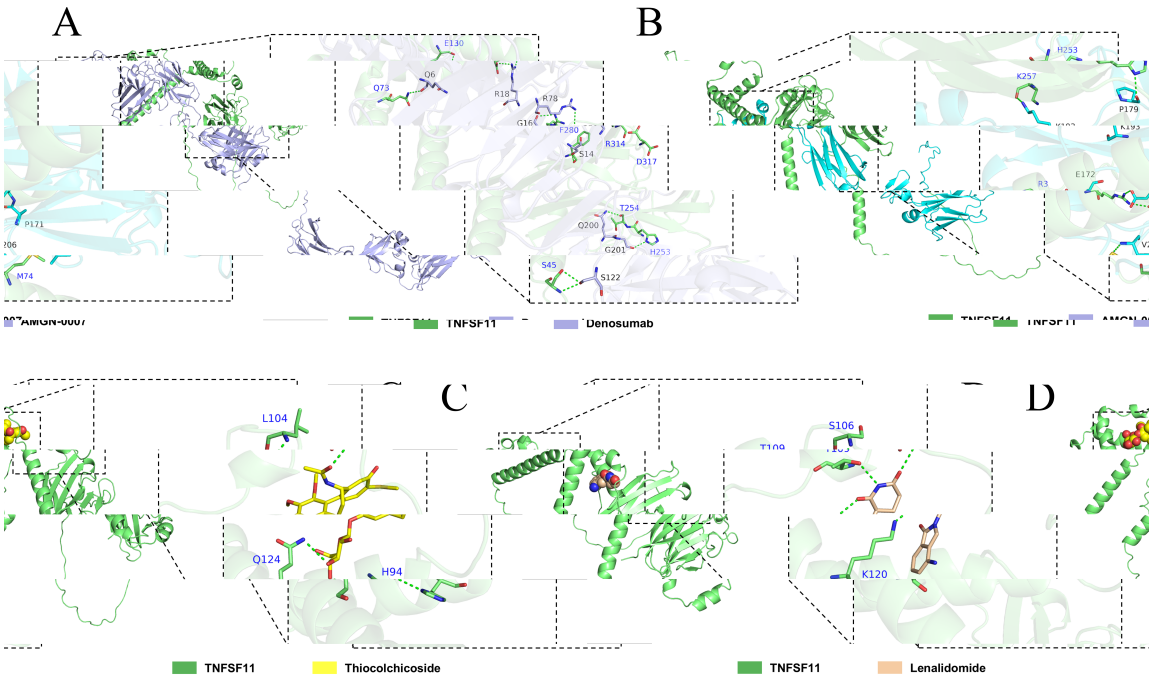

Figure 8. Molecular docking validation of the predicted targeted drugs for TNFSF11. (**A**) The binding mode of Denosumab with TNFSF11. (**B**) The binding mode of AMGN-0007 with TNFSF11. (**C**) The binding mode of Lenalidomide with TNFSF11. (**D**) The binding mode of Thiocolchicoside with TNFSF11.

3.9. Mendelian Randomization and Experimental Validation

To establish causal relationships between TNFSF11 and its target genes with OA susceptibility, we conducted a two-sample Mendelian randomization analysis. The results revealed divergent causal effects among the examined genes (Table 2). Three genes demonstrated protective effects against OA development: CTSK (OR = 0.99902, 95% CI: 0.99826–0.99980, $p = 0.01306$), SPP1 (OR = 0.99724, 95% CI: 0.99565–0.99884, $p = 0.00070$), and TBXAS1 (OR = 0.99767, 95% CI: 0.99570–0.99965, $p = 0.02088$). Conversely, five genes emerged as risk factors for OA. Among these, TNFRSF11A exhibited the strongest causal association (OR = 1.01469, 95% CI: 1.00878–1.02063, $p < 0.00001$), followed by FCGR1A (OR = 1.00817, 95% CI: 1.00414–1.01221, $p = 0.00007$), TNFSF11 (OR = 1.00850, 95% CI: 1.00007–1.01700, $p = 0.04806$), MMP9 (OR = 1.00555, 95% CI: 1.00097–1.01016, $p = 0.01754$), and MMP1 (OR = 1.00464, 95% CI: 1.00138–1.00791, $p = 0.00522$). It should be noted that we found these OR values to be very close to 1, although their p-values were all significant. This suggests potential causal links and clues for further research, rather than definitive evidence of a strong pathogenic effect. While statistically significant in large datasets, their biological or clinical relevance is questionable. Therefore, we further validated them through preliminary experiments.

To experimentally validate these bioinformatic predictions, we performed qRT-PCR analysis on clinically obtained synovial tissue samples. The experimental results corroborated our computational findings, demonstrating significant upregulation of the identified risk factor genes in OA specimens compared to controls. Specifically, TNFRSF11A, FCGR1A, MMP1, MMP9, and TNFSF11 all exhibited significantly elevated mRNA expression levels in osteoarthritic synovium ($p < 0.05$) (Figure 9A–E). This concordance between Mendelian randomization evidence and experimental gene expression data strengthens the validity of our bioinformatics analysis and supports the pathogenic roles of these genes in OA development.

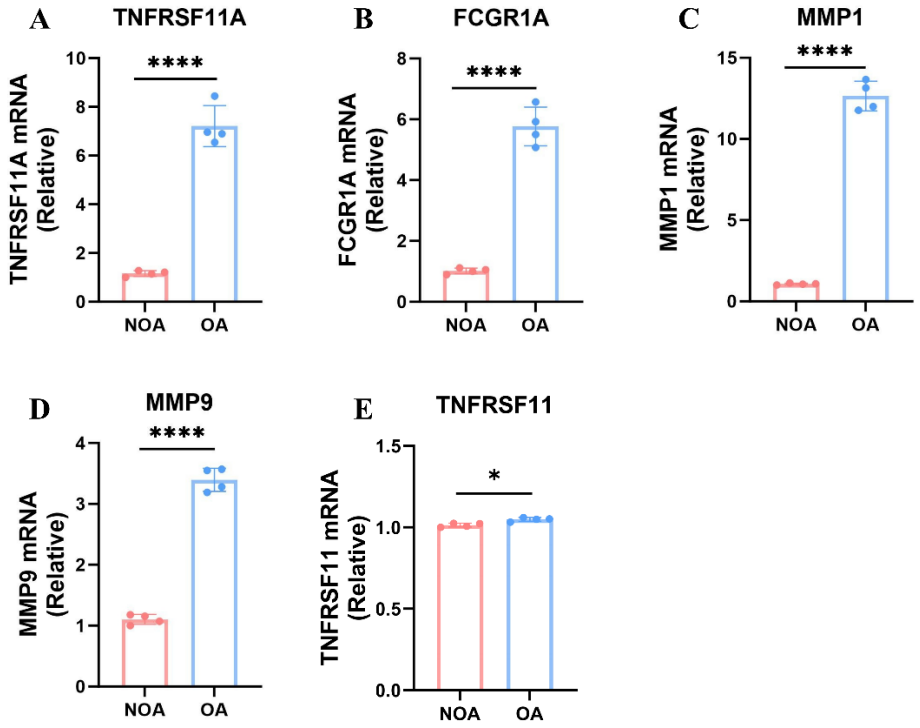

Figure 9. Expression levels of TNFRSF11A, FCGR1A, MMP1, MMP9 and TNFSF11 in CON and OA synovial tissues**.** Relative mRNA expression levels of TNFRSF11A (**A**); FCGR1A (**B**); MMP1 (**C**); MMP9 (**D**); and TNFSF11 (**E**) were determined by quantitative real-time PCR (n = 10 per group). ****$p < 0.0001$, *$p < 0.05$.

Table 2. Causal relationships between genes and OA risk based on mendelian randomization analysis.

Genes	pval	or	or_lci95	or_uci95
BLNK	0.534963326	0.99811222	0.99217208	1.004087923
CD4	0.183538397	0.998587775	0.996510141	1.000669741
CSF1R	0.907296306	1.000107542	0.998299011	1.001919349
CTSK	0.013059179	0.999027387	0.998260044	0.99979532
FCGR1A	6.73E-05	1.008165746	1.004141977	1.012205639
FCGR3A	0.261740001	0.996822123	0.991296377	1.002378671
FCGR3B	0.623541227	0.999557141	0.997790683	1.001326726
MMP1	0.005218774	1.004641504	1.001382305	1.00791131
MMP9	0.017540509	1.005553981	1.000968611	1.010160357
SDC1	0.684137844	0.998124821	0.989139714	1.007191547
SPP1	0.000699754	0.997243706	0.995653412	0.998836541
TBXAS1	0.020875727	0.997673501	0.995703938	0.99964696
TNFRSF11A	9.80E-07	1.014689635	1.00878271	1.020631148
TNFSF11	0.048060698	1.008498393	1.000072055	1.01699573
BLNK	0.534963326	0.99811222	0.99217208	1.004087923
CD4	0.183538397	0.998587775	0.996510141	1.000669741
CSF1R	0.907296306	1.000107542	0.998299011	1.001919349
CTSK	0.013059179	0.999027387	0.998260044	0.99979532

4. Discussion

OA manifests as a chronic progressive joint disorder characterised by irreversible structural alterations encompassing articular cartilage erosion, persistent synovial inflammation, and subchondral bone pathology [46–49]. These degenerative processes culminate in functional impairment and diminished life quality, currently impacting over 230 million individuals globally [50]. The integrative pathogenic framework remains insufficiently characterised.

In this study, we downloaded multiple sets of OA-related transcriptome datasets from the GEO database and utilised R software packages to merge, batch-correct, and normalise the data. Through the Wilcoxon rank-sum test and ROC curve analysis, we found that TNFSF11 was significantly upregulated in OA tissues and had good diagnostic value for OA. Furthermore, we screened gene modules closely related to OA occurrence using differential expression analysis and WGCNA methods and identified 372 candidate genes. Protein interaction

network analysis showed that TNFSF11 can directly interact with 18 targets (BLNK, CD4, CSF1R, CTSK, FCGR1A, FCGR3A, FCGR3B, MMP1, MMP3, MMP9, OGN, SDC1, SPP1, TBXAS1, TNFRSF11A, TYROBP, VCAM-1, TREM2), which are significantly upregulated in OA and positively correlated with TNFSF11 expression. Molecular docking further validated the binding interactions between TNFSF11 and these targets. These findings suggest that TNFSF11 may play a role in the pathogenesis of OA by modulating the expression of downstream target genes. Several identified genes have been shown to possess documented pathological significance in OA. MMP1, MMP3, and MMP9 represent proteolytic enzymes capable of degrading extracellular matrix constituents. Subchondral bone and marrow inflammation has been documented in experimental and clinical arthritis studies [51,52]. In SW1353 chondrosarcoma models, IL-1β stimulation triggers the upregulation of IL-6, PGE2, and COX-2, subsequently activating metalloproteinases, including MMP-1 and MMP-13 [53]. Thus, inflammatory mediators within osteoarthritic cartilage initiate catabolic enzyme cascades culminating in tissue degradation. SPP1 (osteopontin) functions as a pleiotropic cytokine, regulating cellular adhesion, motility, and inflammatory responses, and exhibits elevated expression in diseased cartilage and synovial tissue. TNFRSF11A encodes the RANK receptor, a trimeric transmembrane protein that shares structural homology with the extracellular domain of CD40, a crucial T cell co-stimulatory molecule. RANK transduces TNFSF11 signals that govern osteoclast maturation and functional activation [54].

To further investigate the biological functions involved in the onset and progression of OA mediated by TNFSF11, we performed functional enrichment analysis on genes potentially regulated by TNFSF11 in the PPI network. The results showed that these genes, which directly or indirectly interact with TNFSF11 in OA, were mainly enriched in 20 signalling pathways, including Phagosome, Cell adhesion molecules, Lysosome, Fc gamma R−mediated phagocytosis, NOD-like receptor signalling pathway, and Hematopoietic cell lineage. GSEA analysis confirmed that the expression of multiple KEGG signalling pathways was significantly changed between the OA and CON groups. For example, signalling pathways such as the Phagosome, Cell adhesion molecules, Lysosome, Protein digestion and absorption, Leukocyte transendothelial migration, Hematopoietic cell lineage, and the Intestinal immune network for IgA production were significantly upregulated in osteoarthritic synovial tissue, and this upregulation was considerably more pronounced in osteoarthritic synovial tissue with high TNFSF11 expression. In contrast, signalling pathways such as the Insulin signalling pathway and Regulation of lipolysis in adipocytes were significantly downregulated in osteoarthritic synovial tissue, and this downregulation was even more pronounced in osteoarthritic synovial tissue with high TNFSF11 expression. Among the enriched pathways, cell adhesion molecules (CAMs) play crucial roles in leukocyte trafficking across various inflammatory disorders, including atherosclerosis, rheumatoid arthritis, and OA [55–58]. Notably, VCAM-1 exhibits elevated expression in osteoarthritic synovial fibroblasts, which promotes monocyte recruitment and adhesion [59,60]. Therapeutic reduction of VCAM-1 levels in synovial fluid has been shown to improve the inflammatory environment within OA knee joints [61,62]. These observations indicate that targeting VCAM-1 expression may represent a promising strategy for alleviating OA symptoms. In osteoarthritic joints, aberrant RANKL upregulation triggers disproportionate osteoclastogenesis within the subchondral bone [63]. Enhanced osteoclast activity accelerates bone resorption, compromising structural integrity and disrupting normal biomechanical loading patterns, thereby amplifying cartilage degradation [64].

The infiltration of immune cells exerts a critical influence on the progression of OA, while TNFSF11 functions as a central cytokine that modulates the immune system, including T lymphocytes, B lymphocytes, and macrophages [65–67]. We compared the infiltration differences of these 22 immune cell subsets in the synovial tissue of the OA and CON groups. The results showed that immune cell subsets, including naive B cells, T regulatory (Tregs), M0 macrophages, and resting Mast cells, were significantly upregulated in osteoarthritic synovial tissue, whereas CD4 memory T cells, activated Mast cells, resting NK cells, and Eosinophils were downregulated considerably in osteoarthritic synovial tissue. Furthermore, we investigated the correlation between TNFSF11 expression and the infiltration of these 22 immune cell subsets. The results showed that TNFSF11 expression had a significant negative correlation with the infiltration of CD4 memory resting cells and activated NK cells, and a significant positive correlation with the infiltration of macrophages (M0). Within the synovium of OA, the predominant cellular populations identified are T lymphocytes and macrophages. These cells, alongside activated synovial fibroblasts, contribute to the subsequent synthesis of cytokines and enhanced angiogenic activity, thereby initiating a deleterious feedback loop that triggers the release of metalloproteinases and proteases. This cascade ultimately results in the persistent breakdown of articular cartilage [68–71]. Among the most prevalent immune cell populations within the synovial tissue of OA, macrophages secrete a spectrum of pro-inflammatory cytokines and chemokines. These mediators contribute to the persistence of synovial inflammation, thereby exacerbating OA pathogenesis—for example, through the action of Rspo2 [64]. The immune cell composition data reported here extend current understanding of TNFSF11's role in shaping the OA immune

microenvironment. The significant enrichment of undifferentiated M0 macrophages in OA synovium, coupled with a positive correlation between TNFSF11 expression and M0 abundance, suggests that TNFSF11 may actively recruit or sustain undifferentiated macrophages within the joint, potentially priming them for subsequent M1 polarisation and amplified pro-inflammatory cytokine secretion. Conversely, the depletion of CD4+ memory resting T cells and activated NK cells—both negatively correlated with TNFSF11—implies that elevated TNFSF11 suppresses adaptive immune surveillance and innate cytotoxic activity within the OA joint, a novel observation that warrants mechanistic investigation in dedicated cell-based and animal models.

Given the vital role of TNFSF11 in OA pathogenesis, targeting TNFSF11 may represent a promising therapeutic strategy for OA. Preclinical studies and clinical trials have demonstrated that bisphosphonates, denosumab, or the cathepsin K inhibitor MIV-711 exhibit effective inhibition of osteoclast function in OA [72–79]. Using the DrugBank database, we also predicted four potential drugs that could target TNFSF11, including AMGN-0007, denosumab, lenalidomide, and thiocolchicoside. AMGN-0007 is an investigational anti-RANKL monoclonal antibody that has shown efficacy in reducing bone resorption in postmenopausal women and patients with bone metastases from breast cancer and osteosarcoma [80]. Denosumab is a human monoclonal antibody targeting RANKL, approved for the treatment of osteoporosis and bone metastases [81]. Lenalidomide is an immunomodulatory drug that can downregulate RANKL expression in bone marrow stromal cells and inhibit osteoclastogenesis [82,83]. Thiocolchicoside is a muscle relaxant that has been reported to inhibit RANKL-induced osteoclast differentiation and bone resorption [84,85]. Molecular docking validated the good binding affinities of these drugs with TNFSF11, suggesting their potential as TNFSF11-targeted therapies for OA. However, their efficacy and safety in OA treatment require further investigation in both preclinical and clinical studies.

To summarise, this study utilises a holistic bioinformatics framework to systematically unravel the molecular underpinnings of TNFSF11 in OA pathogenesis through multiple analytical dimensions, encompassing transcriptomic data profiling, weighted gene co-expression network analysis, protein-protein interaction network exploration, molecular docking simulations, functional enrichment assessment, immune infiltration pattern analysis, and drug candidate prediction. The multidimensional regulatory network of TNFSF11 constructed in this study provides a valuable resource and framework for further investigations into the molecular mechanisms and translational applications of TNFSF11 in OA.

Although this study provides valuable insights into the role of TNFSF11 in OA, several limitations should be acknowledged. First, the analyses were primarily based on publicly available transcriptome datasets, which may introduce biases related to sample collection, processing, and population diversity. Second, while bioinformatics methods such as WGCNA and PPI network analysis identified TNFSF11 and its associated gene interactions, these findings lack experimental validation. Functional mechanisms and regulatory interactions inferred from this study need to be confirmed through *in vitro* and *in vivo* models of OA. Third, regarding molecular docking, it should be noted that docking-derived binding energies are approximations and should not be interpreted as experimentally validated thermodynamic parameters. The docking of monoclonal antibodies using HDOCK does not substitute for rigorous structural epitope mapping, and experimental binding validation—such as surface plasmon resonance or isothermal titration calorimetry—is required to confirm the predicted protein–ligand interactions. Fourth, the immune infiltration analysis relied on computational estimation, which may not fully reflect the complexity of the local immune microenvironment in OA joints; direct experimental validation using histological or flow cytometric approaches is therefore warranted. Fifth, although molecular docking suggested potential drugs targeting TNFSF11, their therapeutic efficacy and safety in OA remain unproven and require rigorous preclinical and clinical testing, as computational drug prediction cannot replace experimental pharmacological evaluation. Sixth, the Mendelian randomization analysis yielded odds ratios very close to 1, indicating only small effect sizes; these results should therefore be interpreted as exploratory evidence of potential causal associations rather than definitive proof of a strong pathogenic role of TNFSF11 in OA. Seventh, the clinical validation cohort was limited by relatively low statistical power, which may have compromised the ability to detect modest associations and warrants replication in larger, well-powered independent cohorts. Finally, as OA is a multifactorial disease, other pathways and factors contributing to its pathogenesis may not have been fully captured in this study. Addressing these limitations in future research will be critical for translating these findings into effective diagnostic and therapeutic strategies. Finally, as OA is a multifactorial disease, other pathways and factors contributing to its pathogenesis may not have been fully captured in this study. Addressing these limitations in future research will be critical for translating these findings into effective diagnostic and therapeutic strategies. Our data suggest a model where elevated synovial TNFSF11 effect M0 macrophages and CD4+ memory resting T cells infiltration and upregulates MMP, SPP1, and RANK expression in synovial fibroblasts, creating a feed-forward loop of inflammation and matrix degradation.

The novelty of this study is multi-layered. While the pro-osteoclastogenic role of TNFSF11 is well established, its broader regulatory networks within the OA synovial microenvironment—spanning co-expression modules, direct protein interaction partners, immune infiltration correlates, and causal genetic relationships—remain incompletely characterised. This study is, to our knowledge, the first to apply a fully integrated workflow combining WGCNA, PPI network construction, CIBERSORTx immune deconvolution, and two-sample Mendelian randomisation to systematically map the TNFSF11-centred regulatory landscape in OA synovial tissue. Crucially, the inclusion of Mendelian randomisation moves beyond correlative transcriptomic evidence to provide genetic-level causal inference for the relationships between TNFSF11 and key interactors (TNFRSF11A, FCGR1A, MMP1, MMP9) and OA susceptibility. Furthermore, the identification of three drug candidates not previously evaluated in TNFSF11-targeted OA therapy (AMGN-0007, lenalidomide, thiocolchicoside) opens new avenues for mechanism-guided therapeutic development.

5. Conclusions

To summarize, this study provides comprehensive insights into the molecular mechanisms underlying the role of TNFSF11 in OA development. Our findings demonstrate that TNFSF11 is markedly upregulated in OA synovial tissues and is closely associated with critical processes, including matrix degradation, subchondral bone remodelling, and immune activation. Via integrated bioinformatics analyses, we identified several genes and signaling pathways regulated by TNFSF11—including MMPs, SPP1, and RANK—all of which contribute to the inflammatory and degenerative processes of OA. Furthermore, TNFSF11 expression is positively correlated with immune cell infiltration—particularly that of M0 macrophages and CD4+ memory resting T cells—suggesting its potential role in shaping the local immune microenvironment in OA. We also identified four potential therapeutic agents targeting TNFSF11—namely AMGN-0007, denosumab, lenalidomide, and thiocolchicoside—that may provide new treatment options for OA. However, additional experimental studies and clinical trials are required to validate these findings and assess the safety and efficacy of TNFSF11-targeted therapies. While the present study has certain limitations, our findings highlight TNFSF11 as a promising biomarker and therapeutic target for OA, thereby providing valuable guidance for future research and clinical practice.

Supplementary Materials

The additional data and information can be downloaded at: https://media.sciltp.com/articles/others/26031 91005572559/RMD-26010161-SM.pdf. Table S1: Detailed demographic and clinical data of 20 individual study participants. Table S2: Primer sequences of target genes and endogenous reference gene.

Author Contributions

F.Y. and X.F.: wrote the main manuscript text; X.M. and Y.W. contributed to drafting. F.Y. and X.F.: collected and assembled the data; X.M., X.F., I.P., A.R.S. and X.W.: secured funding. All authors have read and agreed to the published version of the manuscript.

Funding

This research was funded by the Natural Science Foundation of Hunan Province (grant numbers 2023JJ30773 and 2025JJ60480), the Hunan Provincial Health Commission (grant numbers 202204072544, 20255326, and W20243023), the Science and Technology Innovation Program of Hunan Province (grant number 2024RC3053), the NHMRC Investigator Grant Fellowship (grant number APP1176298), the CBT ECR/MCR Scheme (grant number 324910-0028/07), the National Natural Science Foundation of China (grant number 32300652), and the Scientific Research Launch Project for New Employees of the Second Xiangya Hospital of Central South University.

Institutional Review Board Statement

The study was conducted in accordance with the Declaration of Helsinki and was approved by the Ethics Committee of The Second Xiangya Hospital of Central South University (protocol code LYEC2025-0291, approved 29 October 2025).

Informed Consent Statement

Informed consent was obtained from all subjects involved in the study.

Data Availability Statement

The datasets used in this study are accessible in the Gene Expression Omnibus (GEO) database at https://www.ncbi.nlm.nih.gov/geo/, with accession numbers GSE55235, GSE55457, and GSE82107. The tools and databases employed, such as STRING (https://string-db.org/), DAVID (https://david.ncifcrf.gov/), CIBERSORTx (https://cibersortx.stanford.edu/), DrugBank (https://go.drugbank.com/), RCSB Protein Data Bank (https://www.rcsb.org/), and HDOCK server (http://hdock.phys.hust.edu.cn/), are publicly available. All data generated or analysed during this research are included in this article and its supplementary files. The code used can be obtained from the corresponding author upon reasonable request.

Conflicts of Interest

Regarding the role of Young Editorial Board member, Xiwei Fan had no involvement in the peer review of this paper and had no access to information regarding its peer-review process. Full responsibility for the editorial process related to this paper was delegated to another editor of the journal.

Use of AI and AI-Assisted Technologies

No AI tools were utilized for this paper.

Abbreviations

OA	Osteoarthritis
DEGs	Differentially expressed genes
WGCNA	Weighted gene co-expression network analysis
PPI	protein-protein interaction
ECM	extracellular matrix
MMPs	matrix metalloproteinases
TLR	Toll-like receptor
TNFSF11	Tumor necrosis factor superfamily member 11
RANKL	receptor activator of nuclear factor κB ligand
ADAMTS	a disintegrin and metalloproteinase with thrombospondin motifs
WGCNA	weighted gene co-expression network analysis
UMAP	uniform manifold approximation and projection
AUC	area under the curve
MEs	module eigengenes
L-RMSD	ligand root mean square deviation
GSEA	gene set enrichment analysis
NES	normalized enrichment score
BP	biological processes
CC	cellular components
MF	molecular function
Tregs	T cells regulatory
DAMP	damage-associated molecular patterns
NLR	nod-like receptor
OPG	osteoprotegerin
ADAM	a disintegrin and metalloproteinase domain
IL-1β	interleukin-1β
IL-6	interleukin-6
PGE2	prostaglandin E2
Cox-2	cyclooxygenase 2
SPP1	secreted phosphoprotein 1
CAMs	cell adhesion molecules
VCAM-1	vascular cell adhesion molecule-1

References

1. Kulkarni, P.; Martson, A.; Vidya, R.; et al. Pathophysiological Landscape of Osteoarthritis. *Adv. Clin. Chem.* **2021**, *100*, 37–90. https://doi.org/10.1016/bs.acc.2020.04.002.
2. Bannuru, R.R.; Osani, M.C.; Vaysbrot, E.E.; et al. OARSI Guidelines for the Non-Surgical Management of Knee, Hip, and Polyarticular Osteoarthritis. *Osteoarthr. Cartil.* **2019**, *27*, 1578–1589. https://doi.org/10.1016/j.joca.2019.06.011.

3. Fisch, K.M.; Gamini, R.; Alvarez-Garcia, O.; et al. Identification of Transcription Factors Responsible for Dysregulated Networks in Human Osteoarthritis Cartilage by Global Gene Expression Analysis. *Osteoarthr. Cartil.* **2018**, *26*, 1531–1538. https://doi.org/10.1016/j.joca.2018.07.012.
4. Mead, T.J.; Apte, S.S. ADAMTS Proteins in Human Disorders. *Matrix Biol.* **2018**, *71–72*, 225–239. https://doi.org/10.1016/j.matbio.2018.06.002.
5. Milaras, C.; Lepetsos, P.; Dafou, D.; et al. Association of Matrix Metalloproteinase (MMP) Gene Polymorphisms with Knee Osteoarthritis: A Review of the Literature. *Cureus* **2021**, *13*, e18607. https://doi.org/10.7759/cureus.18607.
6. Goldring, M.B.; Otero, M.; Tsuchimochi, K.; et al. Defining the Roles of Inflammatory and Anabolic Cytokines in Cartilage Metabolism. *Ann. Rheum. Dis.* **2008**, *67*, iii75–iii82. https://doi.org/10.1136/ard.2008.098764.
7. Li, S.; Shi, Y.; Zhang, S.; et al. Corynoline Alleviates Osteoarthritis Development via the Nrf2/NF-κB Pathway. *Oxid. Med. Cell. Longev.* **2022**, *2022*, 2188145. https://doi.org/10.1155/2022/2188145.
8. Fazio, A.; Di Martino, A.; Brunello, M.; et al. The Involvement of Signaling Pathways in the Pathogenesis of Osteoarthritis: An Update. *J. Orthop. Transl.* **2024**, *47*, 116–124. https://doi.org/10.1016/j.jot.2024.06.002.
9. Sassi, N.; Laadhar, L.; Driss, M.; et al. The Role of the Notch Pathway in Healthy and Osteoarthritic Articular Cartilage: From Experimental Models to *Ex Vivo* Studies. *Arthritis Res. Ther.* **2011**, *13*, 208. https://doi.org/10.1186/ar3255.
10. Karlsson, C.; Brantsing, C.; Egell, S.; et al. Notch1, Jagged1, and HES5 Are Abundantly Expressed in Osteoarthritis. *Cells Tissues Organs* **2008**, *188*, 287–298. https://doi.org/10.1159/000121610.
11. Hu, X.; Li, J.; Fu, M.; et al. The JAK/STAT Signaling Pathway: From Bench to Clinic. *Signal Transduct. Target. Ther.* **2021**, *6*, 402. https://doi.org/10.1038/s41392-021-00791-1.
12. Zhou, Q.; Ren, Q.; Jiao, L.; et al. The Potential Roles of JAK/STAT Signaling in the Progression of Osteoarthritis. *Front. Endocrinol.* **2022**, *13*, 1069057. https://doi.org/10.3389/fendo.2022.1069057.
13. Lim, H.; Kim, H.P. Matrix Metalloproteinase-13 Expression in IL-1β-Treated Chondrocytes by Activation of the p38 MAPK/c-Fos/AP-1 and JAK/STAT Pathways. *Arch. Pharmacal Res.* **2011**, *34*, 109–117. https://doi.org/10.1007/s12272-011-0113-4.
14. Meszaros, E.C.; Malemud, C.J. Phosphorylation of STAT Proteins by Recombinant Human IL-6 in Immortalized Human Chondrocyte Cell Lines, T/C28a2 and C28/I2. *J. Inflamm. Res.* **2017**, *10*, 143–150. https://doi.org/10.2147/jir.S93797.
15. Xuan, F.; Yano, F.; Mori, D.; et al. Wnt/β-Catenin Signaling Contributes to Articular Cartilage Homeostasis through Lubricin Induction in the Superficial Zone. *Arthritis Res. Ther.* **2019**, *21*, 247. https://doi.org/10.1186/s13075-019-2041-5.
16. Zhou, Y.; Wang, T.; Hamilton, J.L.; et al. Wnt/β-Catenin Signaling in Osteoarthritis and in Other Forms of Arthritis. *Curr. Rheumatol. Rep.* **2017**, *19*, 53. https://doi.org/10.1007/s11926-017-0679-z.
17. Li, K.; Zhang, Y.; Zhang, Y.; et al. Tyrosine Kinase Fyn Promotes Osteoarthritis by Activating the β-Catenin Pathway. *Ann. Rheum. Dis.* **2018**, *77*, 935–943. https://doi.org/10.1136/annrheumdis-2017-212658.
18. Cheng, P.; Wirka, R.C.; Kim, J.B.; et al. Smad3 Regulates Smooth Muscle Cell Fate and Mediates Adverse Remodeling and Calcification of the Atherosclerotic Plaque. *Nat. Cardiovasc. Res.* **2022**, *1*, 322–333. https://doi.org/10.1038/s44161-022-00042-8.
19. Lafyatis, R. Transforming Growth Factor β—At the Centre of Systemic Sclerosis. *Nat. Rev. Rheumatol.* **2014**, *10*, 706–719. https://doi.org/10.1038/nrrheum.2014.137.
20. Pickup, M.; Novitskiy, S.; Moses, H.L. The Roles of TGFβ in the Tumour Microenvironment. *Nat. Rev. Cancer* **2013**, *13*, 788–799. https://doi.org/10.1038/nrc3603.
21. Liu-Bryan, R.; Terkeltaub, R. Emerging Regulators of the Inflammatory Process in Osteoarthritis. *Nat. Rev. Rheumatol.* **2015**, *11*, 35–44. https://doi.org/10.1038/nrrheum.2014.162.
22. Chen, Z.; Zhong, H.; Wei, J.; et al. Inhibition of Nrf2/HO-1 Signaling Leads to Increased Activation of the NLRP3 Inflammasome in Osteoarthritis. *Arthritis Res. Ther.* **2019**, *21*, 300. https://doi.org/10.1186/s13075-019-2085-6.
23. Tudorachi, N.B.; Totu, E.E.; Fifere, A.; et al. The Implication of Reactive Oxygen Species and Antioxidants in Knee Osteoarthritis. *Antioxidants* **2021**, *10*, 985. https://doi.org/10.3390/antiox10060985.
24. Lepetsos, P.; Papavassiliou, K.A.; Papavassiliou, A.G. Redox and NF-κB Signaling in Osteoarthritis. *Free Radical Biol. Med.* **2019**, *132*, 90–100. https://doi.org/10.1016/j.freeradbiomed.2018.09.025.
25. Bolduc, J.A.; Collins, J.A.; Loeser, R.F. Reactive Oxygen Species, Aging and Articular Cartilage Homeostasis. *Free Radic. Biol. Med.* **2019**, *132*, 73–82. https://doi.org/10.1016/j.freeradbiomed.2018.08.038.
26. Li, J.; Jiang, M.; Yu, Z.; et al. Artemisinin Relieves Osteoarthritis by Activating Mitochondrial Autophagy through Reducing TNFSF11 Expression and Inhibiting PI3K/AKT/mTOR Signaling in Cartilage. *Cell. Mol. Biol. Lett.* **2022**, *27*, 62. https://doi.org/10.1186/s11658-022-00365-1.
27. Sun, Z.; Liu, Q.; Lv, Z.; et al. Targeting Macrophagic SHP2 for Ameliorating Osteoarthritis via TLR Signaling. *Acta Pharm. Sin. B* **2022**, *12*, 3073–3084. https://doi.org/10.1016/j.apsb.2022.02.010.
28. Kloppenburg, M.; Berenbaum, F. Osteoarthritis Year in Review 2019: Epidemiology and Therapy. *Osteoarthritis Cartilage* **2020**, *28*, 242–248. https://doi.org/10.1016/j.joca.2020.01.002.

29. Zeng, X.Z.; He, L.G.; Wang, S.; et al. Aconine Inhibits RANKL-Induced Osteoclast Differentiation in RAW264.7 Cells by Suppressing NF-κB and NFATc1 Activation and DC-STAMP Expression. *Acta Pharmacol. Sin.* **2016**, *37*, 255–263. https://doi.org/10.1038/aps.2015.85.
30. Bonnet, N.; Bourgoin, L.; Biver, E.; et al. RANKL Inhibition Improves Muscle Strength and Insulin Sensitivity and Restores Bone Mass. *J. Clin. Invest.* **2019**, *129*, 3214–3223. https://doi.org/10.1172/jci125915.
31. Yan, M.; Su, J.; Li, Y. Rheumatoid Arthritis-Associated Bone Erosions: Evolving Insights and Promising Therapeutic Strategies. *BioSci. Trends* **2020**, *14*, 342–348. https://doi.org/10.5582/bst.2020.03253.
32. Yue, Z.; Niu, X.; Yuan, Z.; et al. RSPO2 and RANKL Signal through LGR4 to Regulate Osteoclastic Premetastatic Niche Formation and Bone Metastasis. *J. Clin. Invest.* **2022**, *132*, e144579. https://doi.org/10.1172/jci144579.
33. Chen, Z.; Wang, W.; Zhang, Y.; et al. Identification of Four-Gene Signature to Diagnose Osteoarthritis through Bioinformatics and Machine Learning Methods. *Cytokine* **2023**, *169*, 156300. https://doi.org/10.1016/j.cyto.2023.156300.
34. Kovács, B.; Vajda, E.; Nagy, E.E. Regulatory Effects and Interactions of the Wnt and OPG-RANKL-RANK Signaling at the Bone-Cartilage Interface in Osteoarthritis. *Int. J. Mol. Sci.* **2019**, *20*, 4653. https://doi.org/10.3390/ijms20184653.
35. Danks, L.; Komatsu, N.; Guerrini, M.M.; et al. RANKL Expressed on Synovial Fibroblasts Is Primarily Responsible for Bone Erosions during Joint Inflammation. *Ann. Rheum. Dis.* **2016**, *75*, 1187–1195. https://doi.org/10.1136/annrheumdis-2014-207137.
36. Parkin, J.; Cohen, B. An Overview of the Immune System. *Lancet* **2001**, *357*, 1777–1789. https://doi.org/10.1016/s0140-6736(00)04904-7.
37. Luo, P.; Yuan, Q.; Wan, X.; et al. Effects of Immune Cells and Cytokines on Different Cells in OA. *J. Inflamm. Res.* **2023**, *16*, 2329–2343. https://doi.org/10.2147/jir.S413578.
38. Goldring, M.B.; Otero, M. Inflammation in Osteoarthritis. *Curr. Opin. Rheumatol.* **2011**, *23*, 471–478. https://doi.org/10.1097/BOR.0b013e328349c2b1.
39. Yan, Y.; Tao, H.; He, J.; et al. The HDOCK Server for Integrated Protein-Protein Docking. *Nat. Protoc.* **2020**, *15*, 1829–1852. https://doi.org/10.1038/s41596-020-0312-x.
40. Lu, J.; Hu, D.; Zhang, Y.; et al. Current Comprehensive Understanding of Denosumab (The RANKL Neutralizing Antibody) in the Treatment of Bone Metastasis of Malignant Tumors, Including Pharmacological Mechanism and Clinical Trials. *Front. Oncol.* **2023**, *13*, 1133828. https://doi.org/10.3389/fonc.2023.1133828.
41. Lacey, D.L.; Boyle, W.J.; Simonet, W.S.; et al. Bench to Bedside: Elucidation of the OPG-RANK-RANKL Pathway and the Development of Denosumab. *Nat. Rev. Drug Discov.* **2012**, *11*, 401–419. https://doi.org/10.1038/nrd3705.
42. Kostenuik, P.J.; Nguyen, H.Q.; McCabe, J.; et al. Denosumab, a Fully Human Monoclonal Antibody to RANKL, Inhibits Bone Resorption and Increases BMD in Knock-In Mice That Express Chimeric (Murine/Human) RANKL. *J. Bone Miner. Res.* **2009**, *24*, 182–195. https://doi.org/10.1359/jbmr.081112.
43. Dougall, W.C.; Holen, I.; González Suárez, E. Targeting RANKL in Metastasis. *BoneKEy Rep.* **2014**, *3*, 519. https://doi.org/10.1038/bonekey.2014.14.
44. Chiu, Y.G.; Ritchlin, C.T. Denosumab: Targeting the RANKL Pathway to Treat Rheumatoid Arthritis. *Expert Opin. Biol. Ther.* **2017**, *17*, 119–128. https://doi.org/10.1080/14712598.2017.1263614.
45. Bone, H.G.; Chapurlat, R.; Brandi, M.L.; et al. The Effect of Three or Six Years of Denosumab Exposure in Women with Postmenopausal Osteoporosis: Results from the FREEDOM Extension. *J. Clin. Endocrinol. Metab.* **2013**, *98*, 4483–4492. https://doi.org/10.1210/jc.2013-1597.
46. Huang, J.G.; Xia, C.; Zheng, X.P.; et al. 17β-Estradiol Promotes Cell Proliferation in Rat Osteoarthritis Model Chondrocytes via PI3K/Akt Pathway. *Cell. Mol. Biol. Lett.* **2011**, *16*, 564–575. https://doi.org/10.2478/s11658-011-0023-y.
47. Abramoff, B.; Caldera, F.E. Osteoarthritis: Pathology, Diagnosis, and Treatment Options. *Med. Clin. North Am.* **2020**, *104*, 293–311. https://doi.org/10.1016/j.mcna.2019.10.007.
48. Peat, G.; Thomas, M.J. Osteoarthritis Year in Review 2020: Epidemiology & Therapy. *Osteoarthr. Cartil.* **2021**, *29*, 180–189. https://doi.org/10.1016/j.joca.2020.10.007.
49. Li, J.; Jiang, M.; Xiong, C.; et al. KLF4, Negatively Regulated by miR-7, Suppresses Osteoarthritis Development via Activating TGF-β1 Signaling. *Int. Immunopharmacol.* **2022**, *102*, 108416. https://doi.org/10.1016/j.intimp.2021.108416.
50. Mandl, L.A. Osteoarthritis Year in Review 2018: Clinical. *Osteoarthr. Cartil.* **2019**, *27*, 359–364. https://doi.org/10.1016/j.joca.2018.11.001.
51. Yu, D.; Xu, J.; Liu, F.; et al. Subchondral Bone Changes and the Impacts on Joint Pain and Articular Cartilage Degeneration in Osteoarthritis. *Clin. Exp. Rheumatol.* **2016**, *34*, 929–934.
52. Nagy, E.; Vajda, E.; Vari, C.; et al. Meloxicam Ameliorates the Cartilage and Subchondral Bone Deterioration in Monoiodoacetate-Induced Rat Osteoarthritis. *PeerJ* **2017**, *5*, e3185. https://doi.org/10.7717/peerj.3185.
53. Shi, J.; Schmitt-Talbot, E.; DiMattia, D.A.; et al. The Differential Effects of IL-1 and TNF-Alpha on Proinflammatory Cytokine and Matrix Metalloproteinase Expression in Human Chondrosarcoma Cells. *Inflamm. Res.* **2004**, *53*, 377–389. https://doi.org/10.1007/s00011-004-1271-3.

54. Anderson, D.M.; Maraskovsky, E.; Billingsley, W.L.; et al. A Homologue of the TNF Receptor and Its Ligand Enhance T-Cell Growth and Dendritic-Cell Function. *Nature* **1997**, *390*, 175–179. https://doi.org/10.1038/36593.
55. Li, Q.; Liu, J.; Liu, W.; et al. LOX-1 Regulates *P. gingivalis*-Induced Monocyte Migration and Adhesion to Human Umbilical Vein Endothelial Cells. *Front. Cell Dev. Biol.* **2020**, *8*, 596. https://doi.org/10.3389/fcell.2020.00596.
56. Manning, J.E.; Lewis, J.W.; Marsh, L.J.; et al. Insights into Leukocyte Trafficking in Inflammatory Arthritis—Imaging the Joint. *Front. Cell Dev. Biol.* **2021**, *9*, 635102. https://doi.org/10.3389/fcell.2021.635102.
57. Pezhman, L.; Tahrani, A.; Chimen, M. Dysregulation of Leukocyte Trafficking in Type 2 Diabetes: Mechanisms and Potential Therapeutic Avenues. *Front. Cell Dev. Biol.* **2021**, *9*, 624184. https://doi.org/10.3389/fcell.2021.624184.
58. Law, Y.Y.; Lin, Y.M.; Liu, S.C.; et al. Visfatin Increases ICAM-1 Expression and Monocyte Adhesion in Human Osteoarthritis Synovial Fibroblasts by Reducing miR-320a Expression. *Aging* **2020**, *12*, 18635–18648. https://doi.org/10.18632/aging.103889.
59. Xiao, S.; Tang, Y.; Lin, Y.; et al. Tracking Osteoarthritis Progress through Cationic Nanoprobe-Enhanced Photoacoustic Imaging of Cartilage. *Acta Biomater.* **2020**, *109*, 153–162. https://doi.org/10.1016/j.actbio.2020.04.001.
60. Han, D.; Fang, Y.; Tan, X.; et al. The Emerging Role of Fibroblast-like Synoviocytes-Mediated Synovitis in Osteoarthritis: An Update. *J. Cell. Mol. Med.* **2020**, *24*, 9518–9532. https://doi.org/10.1111/jcmm.15669.
61. Liu, J.F.; Hou, S.M.; Tsai, C.H.; et al. CCN4 Induces Vascular Cell Adhesion Molecule-1 Expression in Human Synovial Fibroblasts and Promotes Monocyte Adhesion. *Biochim. Biophys. Acta Mol. Cell Res.* **2013**, *1833*, 966–975. https://doi.org/10.1016/j.bbamcr.2012.12.023.
62. Yang, C.R.; Shih, K.S.; Liou, J.P.; et al. Denbinobin Upregulates miR-146a Expression and Attenuates IL-1β-Induced Upregulation of ICAM-1 and VCAM-1 Expressions in Osteoarthritis Fibroblast-like Synoviocytes. *J. Mol. Med.* **2014**, *92*, 1147–1158. https://doi.org/10.1007/s00109-014-1192-8.
63. Bertuglia, A.; Lacourt, M.; Girard, C.; et al. Osteoclasts Are Recruited to the Subchondral Bone in Naturally Occurring Post-Traumatic Equine Carpal Osteoarthritis and May Contribute to Cartilage Degradation. *Osteoarthr. Cartil.* **2016**, *24*, 555–566. https://doi.org/10.1016/j.joca.2015.10.008.
64. Yan, J.Y.; Tian, F.M.; Wang, W.Y.; et al. Parathyroid Hormone (1–34) Prevents Cartilage Degradation and Preserves Subchondral Bone Micro-Architecture in Guinea Pigs with Spontaneous Osteoarthritis. *Osteoarthr. Cartil.* **2014**, *22*, 1869–1877. https://doi.org/10.1016/j.joca.2014.07.013.
65. Tan, W.; Zhang, W.; Strasner, A.; et al. Tumour-Infiltrating Regulatory T Cells Stimulate Mammary Cancer Metastasis through RANKL-RANK Signalling. *Nature* **2011**, *470*, 548–553. https://doi.org/10.1038/nature09707.
66. Titanji, K. Beyond Antibodies: B Cells and the OPG/RANK-RANKL Pathway in Health, Non-HIV Disease and HIV-Induced Bone Loss. *Front. Immunol.* **2017**, *8*, 1851. https://doi.org/10.3389/fimmu.2017.01851.
67. Camara, A.; Cordeiro, O.G.; Alloush, F.; et al. Lymph Node Mesenchymal and Endothelial Stromal Cells Cooperate via the RANK-RANKL Cytokine Axis to Shape the Sinusoidal Macrophage Niche. *Immunity* **2019**, *50*, 1467–1481.e6. https://doi.org/10.1016/j.immuni.2019.05.008.
68. Prieto-Potin, I.; Largo, R.; Roman-Blas, J.A.; et al. Characterization of Multinucleated Giant Cells in Synovium and Subchondral Bone in Knee Osteoarthritis and Rheumatoid Arthritis. *BMC Musculoskelet. Disord.* **2015**, *16*, 226. https://doi.org/10.1186/s12891-015-0664-5.
69. Wojdasiewicz, P.; Poniatowski, Ł.A.; Szukiewicz, D. The Role of Inflammatory and Anti-Inflammatory Cytokines in the Pathogenesis of Osteoarthritis. *Mediat. Inflamm.* **2014**, *2014*, 561459. https://doi.org/10.1155/2014/561459.
70. Klein-Wieringa, I.R.; de Lange-Brokaar, B.J.; Yusuf, E.; et al. Inflammatory Cells in Patients with Endstage Knee Osteoarthritis: A Comparison between the Synovium and the Infrapatellar Fat Pad. *J. Rheumatol.* **2016**, *43*, 771–778. https://doi.org/10.3899/jrheum.151068.
71. Kapoor, M.; Martel-Pelletier, J.; Lajeunesse, D.; et al. Role of Proinflammatory Cytokines in the Pathophysiology of Osteoarthritis. *Nat. Rev. Rheumatol.* **2011**, *7*, 33–42. https://doi.org/10.1038/nrrheum.2010.196.
72. Xu, L.; Hu, Y.J.; Peng, Y.; et al. Early Zoledronate Treatment Inhibits Subchondral Bone Microstructural Changes in Skeletally-Mature, ACL-Transected Canine Knees. *Bone* **2023**, *167*, 116638. https://doi.org/10.1016/j.bone.2022.116638.
73. Ziemian, S.N.; Witkowski, A.M.; Wright, T.M.; et al. Early Inhibition of Subchondral Bone Remodeling Slows Load-Induced Posttraumatic Osteoarthritis Development in Mice. *J. Bone Miner. Res.* **2021**, *36*, 2027–2038. https://doi.org/10.1002/jbmr.4397.
74. Neogi, T.; Li, S.; Peloquin, C.; et al. Effect of Bisphosphonates on Knee Replacement Surgery. *Ann. Rheum. Dis.* **2018**, *77*, 92–97. https://doi.org/10.1136/annrheumdis-2017-211811.
75. Laslett, L.L.; Kingsbury, S.R.; Hensor, E.M.; et al. Effect of Bisphosphonate Use in Patients with Symptomatic and Radiographic Knee Osteoarthritis: Data from the Osteoarthritis Initiative. *Ann. Rheum. Dis.* **2014**, *73*, 824–830. https://doi.org/10.1136/annrheumdis-2012-202989.
76. Kadri, A.; Funck-Brentano, T.; Lin, H.; et al. Inhibition of Bone Resorption Blunts Osteoarthritis in Mice with High Bone Remodelling. *Ann. Rheum. Dis.* **2010**, *69*, 1533–1538. https://doi.org/10.1136/ard.2009.124586.

77. Bihlet, A.R.; Byrjalsen, I.; Andersen, J.R.; et al. Symptomatic and Structural Benefit of Cathepsin K Inhibition by MIV-711 in a Subgroup with Unilateral Pain: Post-Hoc Analysis of a Randomised Phase 2a Clinical Trial. *Clin. Exp. Rheumatol.* **2022**, *40*, 1034–1037. https://doi.org/10.55563/clinexprheumatol/1kvgte.
78. Conaghan, P.G.; Bowes, M.A.; Kingsbury, S.R.; et al. Disease-Modifying Effects of a Novel Cathepsin K Inhibitor in Osteoarthritis: A Randomized Controlled Trial. *Ann. Intern. Med.* **2020**, *172*, 86–95. https://doi.org/10.7326/m19-0675.
79. Lindström, E.; Rizoska, B.; Tunblad, K.; et al. The Selective Cathepsin K Inhibitor MIV-711 Attenuates Joint Pathology in Experimental Animal Models of Osteoarthritis. *J. Transl. Med.* **2018**, *16*, 56. https://doi.org/10.1186/s12967-018-1425-7.
80. Body, J.J.; Greipp, P.; Coleman, R.E.; et al. A Phase I Study of AMGN-0007, a Recombinant Osteoprotegerin Construct, in Patients with Multiple Myeloma or Breast Carcinoma Related Bone Metastases. *Cancer* **2003**, *97*, 887–892. https://doi.org/10.1002/cncr.11138.
81. Di Lorenzo, L. Denosumab in Elderly Osteoporotic Patients. A Narrative Review. *Clin. Ter.* **2023**, *174*, 545–549. https://doi.org/10.7417/ct.2023.5023.
82. Wang, Y.; Xu, J.; Zhang, X.; et al. TNF-α-Induced LRG1 Promotes Angiogenesis and Mesenchymal Stem Cell Migration in the Subchondral Bone during Osteoarthritis. *Cell Death Dis.* **2017**, *8*, e2715. https://doi.org/10.1038/cddis.2017.129.
83. Weisel, K.; Kanz, L. Lenalidomide. *Recent Results Cancer Res.* **2014**, *201*, 347–357. https://doi.org/10.1007/978-3-642-54490-3_21.
84. Reuter, S.; Gupta, S.C.; Phromnoi, K.; et al. Thiocolchicoside Suppresses Osteoclastogenesis Induced by RANKL and Cancer Cells through Inhibition of Inflammatory Pathways: A New Use for an Old Drug. *Br. J. Pharmacol.* **2012**, *165*, 2127–2139. https://doi.org/10.1111/j.1476-5381.2011.01702.x.
85. Yan, Y.; Zhang, D.; Zhou, P.; et al. HDOCK: A Web Server for Protein-Protein and Protein-DNA/RNA Docking Based on a Hybrid Strategy. *Nucleic Acids Res.* **2017**, *45*, w365–w373. https://doi.org/10.1093/nar/gkx407.